

Article

Influence of Oxygen Carrier on the Autothermicity of a Chemical-Looping Reforming Process for Hydrogen Production

Juliana López van der Horst^{1,2}, Maria Florencia Volpe Giangiordano^{1,2}, Felipe Suarez², Federico M. Perez^{1,2}, Martín N. Gatti^{1,2} , Gerardo F. Santori^{1,2} and Francisco Pompeo^{1,2,*} 

¹ Centro de Investigación y Desarrollo en Ciencias Aplicadas (CINDECA), Facultad de Ciencias Exactas, Universidad Nacional de La Plata (UNLP)—CONICET, Calle 47, 257, La Plata 1900, Argentina; julianalopezvdh@quimica.unlp.edu.ar (J.L.v.d.H.); florenciavolpeg@quimica.unlp.edu.ar (M.F.V.G.); federico.perez@ing.unlp.edu.ar (F.M.P.); martin.gatti@ing.unlp.edu.ar (M.N.G.); santori@quimica.unlp.edu.ar (G.F.S.)

² Departamento de Ingeniería Química, Facultad de Ingeniería, Universidad Nacional de La Plata (UNLP), Calle 1 esq. 47, La Plata 1900, Argentina; felipe.suarez@ing.unlp.edu.ar

* Correspondence: fpompeo@quimica.unlp.edu.ar

Abstract: The chemical-looping reforming (CLR) of methane for hydrogen production employs a solid oxygen carrier (OC) and combines endothermic and exothermic stages, allowing for potential autothermal operation. This study conducted a thermodynamic analysis using Gibbs free energy minimization and energy balances to assess the behavior of WO_3 , MnWO_4 , and NiWO_4 as OCs in the CLR process. The effects of CH_4 :OC ratios and reactor temperatures on equilibrium composition and the energy performance were examined. The results demonstrated that elevated reduction temperatures promote OC conversion and the formation of more reduced solid products. Molar ratios above stoichiometric prevent carbon formation, whereas stoichiometric ratios result in higher H_2 yield, achieving 98% at 1000 °C. However, these conditions do not support autothermal operation, which requires CH_4 :OC molar ratios above stoichiometric. Additionally, lower oxidation temperatures are preferred regardless of the OC, due to the lower heat needed to preheat the air, which has a greater effect on the net heat. For the reduction temperature, its effect depends on the type of OC analyzed. The maximum H_2 yield obtained under autothermal operation was 88% for the three OCs, at 875 °C for MnWO_4 and 775 °C for both WO_3 and NiWO_4 .

Keywords: chemical-looping reforming; oxygen carrier; hydrogen; thermodynamics; autothermal



Academic Editor: Wenping Ma

Received: 18 October 2024

Revised: 12 December 2024

Accepted: 1 January 2025

Published: 4 January 2025

Citation: López van der Horst, J.; Volpe Giangiordano, M.F.; Suarez, F.; Perez, F.M.; Gatti, M.N.; Santori, G.F.; Pompeo, F. Influence of Oxygen Carrier on the Autothermicity of a Chemical-Looping Reforming Process for Hydrogen Production. *Reactions* **2025**, *6*, 5. <https://doi.org/10.3390/reactions6010005>

Copyright: © 2025 by the authors. Licensee MDPI, Basel, Switzerland. This article is an open access article distributed under the terms and conditions of the Creative Commons Attribution (CC BY) license (<https://creativecommons.org/licenses/by/4.0/>).

1. Introduction

Currently, syngas and hydrogen are widely used as feedstocks in the synthesis of ammonia, fertilizers, methanol, and in a wide range of industries, including steel, electronics, refining, and petrochemicals, among others. In recent years, however, hydrogen has emerged as a key element in the development of sustainable energy systems to reduce greenhouse gas emissions and environmental contamination. As a clean fuel, hydrogen can be employed to generate both heat and electricity without emitting CO_2 , thus supporting the decarbonization of industry, transportation, heating, and electricity generation. Hydrogen has the potential to reduce dependence on fossil fuels due to its high energy density. Its combustion provides approximately three times more energy per unit mass compared to gasoline, making it a promising alternative energy source [1]. Moreover, hydrogen finds applications in fuel cell technology, constituting an opportunity to fortify diverse

economic sectors [2]. Its ability to act as an energy carrier makes it possible to store energy produced at specific times and places, and to use this energy in a controlled manner at a later stage [3,4]. Furthermore, hydrogen has the potential to serve as a storage medium for renewable energy (referred to as “Power-to-Hydrogen”) [4,5], facilitating the decoupling of energy generation from consumption. Additionally, hydrogen can be produced locally from a wide range of substances, including water, petroleum, natural gas, biofuels, and biomass waste, thereby reducing countries’ dependence on external energy suppliers [1,6].

Although hydrogen is positioned as a crucial element in the transition to clean energy, its environmental performance is largely determined by the feedstock and the process used to produce it, as it is a secondary energy source. By 2021, approximately 47% of global hydrogen production was derived from natural gas, 27% from coal, 22% from oil (as a byproduct), and only 4% from water electrolysis (with only 33% of electricity coming from renewable resources) [7]. This indicates that fossil fuels remain the primary source of hydrogen, with methane being particularly notable due to its high H/C ratio and lower byproduct generation compared to other hydrocarbons [8,9]. In order to achieve a sustainable and environmentally responsible energy matrix in the future, it is essential to invest in the production of hydrogen obtained from renewable energy sources. However, in order to facilitate the energy transition, it is crucial for regions with natural gas reservoirs or potential biogas production to identify alternative methods for utilizing these primary sources to produce hydrogen, while minimizing gas emissions. In this context, low-carbon hydrogen represents an economically viable and advantageous strategy that, when combined with technologies designed to reduce CO₂ emissions, acts as a transition pathway towards a low-carbon economy, taking advantage of existing infrastructure. This represents a lower cost compared to green hydrogen and increases energy diversity, thereby strengthening the energy system and providing additional options to meet growing energy demand.

Achieving optimal, reliable, cost-effective, environmentally sustainable, and efficient hydrogen production presents a complex challenge, as no single method can meet all these goals simultaneously. Since hydrogen does not occur naturally and must be synthesized, there is an urgent need to innovate production techniques that use less energy and enable large-scale manufacturing [6]. Despite the non-renewable nature of the feedstock, implementing carbon capture at the production source enables the decentralized use of hydrogen as a clean fuel for transportation, power generation, and both domestic and industrial heating. Consequently, considerable efforts have been made to identify alternative technologies that promote more efficient hydrogen production, with the aim of reducing energy consumption, decreasing pollutant emissions, and improving process safety.

In this scenario, chemical-looping reforming (CLR) is proposed as an alternative to traditional methane reforming. Compared to conventional reforming, which represents approximately 50% of the world’s hydrogen production [10], the chemical-looping strategy provides an alternative route for methane partial oxidation that avoids contact between the fuel and gaseous oxidants, thus enhancing the operational safety of the process [11]. Instead, in chemical-looping reforming, lattice oxygen of an oxygen carrier (OC) is used to partially oxidize methane to syngas [12]. The oxygen carrier is then re-oxidated using different regeneration agents, such as air or water. This system consists of two fluidized bed reactors through which the oxygen carrier is circulated. In this scheme, the oxygen carrier acts both as an oxygen donor for methane oxidation and as a catalyst to facilitate methane conversion towards syngas, so it differs from a typical heterogeneous redox catalyst, since it is part of the redox reactions. The main advantages of the CLR approach include the elimination of the energy-intensive air separation or steam generation unit and the inherent separation of CO₂ from the exhaust gas, which would facilitate the adoption of capture techniques or its subsequent use. Moreover, since the reduction of the oxygen

carrier is an endothermic reaction, while its regeneration is highly exothermic, the ability to achieve autothermal operation by adjusting the reaction conditions presents a significant advantage over conventional methane reforming for hydrogen production, where high reaction temperatures are achieved by the addition of external heat.

In general, oxygen carriers are metal oxides capable of reacting through their lattice oxygen in reducing atmospheres and subsequently re-oxidizing to regenerate the original material. In order for a material to be considered an attractive option as an OC in CLR, it must present certain general characteristics [11,13,14]:

- High oxygen-carrying storage and availability: the diffusion of lattice oxygen from the bulk phase plays a crucial role in reaction kinetics in CLR processes. Consequently, the oxygen-carrying capacity and the strength of the metal–oxygen bond significantly influence the selectivity of the final products.
- Chemical and structural (or mechanical) stability at elevated temperatures. This implies, for example, having high melting points.
- Favorable thermodynamics regarding reduction and oxidation reactions.
- Favorable kinetics and high selectivity towards syngas formation with minimal byproduct generation, including carbon deposition.
- Regenerability: the material must be easily re-oxidized by a suitable oxidizing agent (e.g., air or water), allowing multiple redox cycles with minimal loss in physical integrity and chemical reactivity.
- Adequate oxidation and reduction reaction enthalpies, so that autothermicity can be achieved in the process.
- Durability over multiple cycles: the OCs must maintain their activity and stability after several redox reduction–oxidation cycles, showing minimal fragmentation, attrition, agglomeration, or other mechanical and thermal degradation. It should also tolerate contaminants.
- Low cost and environmentally friendly.

This work focuses on the thermodynamic study of three materials based on tungsten oxides: MnWO_4 , NiWO_4 , and WO_3 . These solids present characteristics that make them promising candidates for use as oxygen carriers in CLR processes. Notably, their structure provides mechanical strength and excellent chemical stability under various redox atmospheres at high temperatures. In the literature, several oxides (Fe_3O_4 , ZnO , In_2O_3 , SnO_2 , CeO_2 , ZrO_2 , V_2O_5 , MoO_3 , and WO_3) have been studied for methane reforming combined with metal oxide reduction at temperatures below 1000 °C [15,16]. In these works, WO_3 has been reported as one of the most reactive among the metal oxide redox systems studied, and this is mainly attributed to the outstanding resistance to sintering due to its high melting point, which is directly related to its high stability during redox cycling [16–18]. In addition, tungsten oxides are abundant in the earth, their composition is highly tunable, they exhibit good physical stability [18,19], and their thermodynamic properties, according to their location in the adapted Ellingham diagram, show that tungsten oxides have high syngas selectivity, which makes them suitable for CLR [20]. Thermodynamic calculations have demonstrated that these oxides exhibit high selectivity for syngas. However, they also present challenges such as low reducibility, limited reactivity with methane, and the necessity of high reaction temperatures. Therefore, enhancing the lattice oxygen availability and improving methane conversion are two critical aspects that require attention in tungsten oxides.

A reported strategy to address these challenges is the incorporation of additional species to modify the lattice and surface properties of these materials. This approach aims to weaken the W–O bond, thereby increasing the availability of lattice oxygen and enhancing methane activation [21]. Mixed metal oxides, in particular, have been extensively studied

in chemical-looping schemes due to their ability to improve reactivity, mechanical strength, and syngas selectivity while minimizing carbon deposition [13]. By combining different ions, these materials offer tailored oxygen potentials through the synergistic effects of their metal constituents, exhibiting enhanced oxygen mobility, greater oxygen storage capacity, and improved thermal stability compared to monometallic oxides. Furthermore, mixed metal oxides offer superior thermodynamic properties for partial oxidation processes [14].

Many inorganic oxides, especially those from the transition metals, have been evaluated as potential oxygen carriers [22]. Among the studied materials, nickel-based oxygen carriers [13,23–27] stand out as the most extensively studied for methane reforming, primarily because of their high reactivity and stability under severe reaction conditions. Nickel's exceptional activity is attributed to its ability to break C-C bonds; however, this advantage is tempered by significant carbon deposition on the material's surface, which can affect its reducibility. In contrast, manganese-based materials bring complementary advantages. Manganese is recognized for its high oxygen storage capacity and resistance to agglomeration at elevated temperatures [8]. Its oxides are highly active in various oxidation and reduction reactions and are effective catalysts for methane oxidation [28]. Notably, manganese has been reported to enhance the redox properties of catalysts by improving the mobility of surface and lattice oxygen and facilitating the exchange between gaseous and lattice oxygen. This behavior significantly contributes to the activation of molecular oxygen and enhances the material's performance [29–31]. By integrating nickel and manganese into tungsten-based systems, it is possible to take advantage of the synergistic properties of these elements, optimizing the oxygen carrier's performance in chemical-looping reforming.

As previously mentioned, a key requirement that an oxygen carrier must fulfill to be suitable for use in chemical-looping reforming processes is its ability to react effectively with the fuel and exhibit selectivity towards syngas. This performance must be supported by both thermodynamic and kinetic considerations, ensuring that the reaction pathways favor syngas formation while minimizing undesired side reactions. Within this framework, the present study aims to thermodynamically analyze and compare the use of the single oxide WO_3 and two mixed oxides, MnWO_4 and NiWO_4 , as oxygen carriers for chemical-looping reforming. To achieve this objective, their performance was studied under various reaction conditions to identify those that facilitate high H_2 production. Additionally, OCs must present suitable properties that enable autothermal operation. In this regard, energy balances were incorporated to evaluate the conditions under which the process can operate without external heat input.

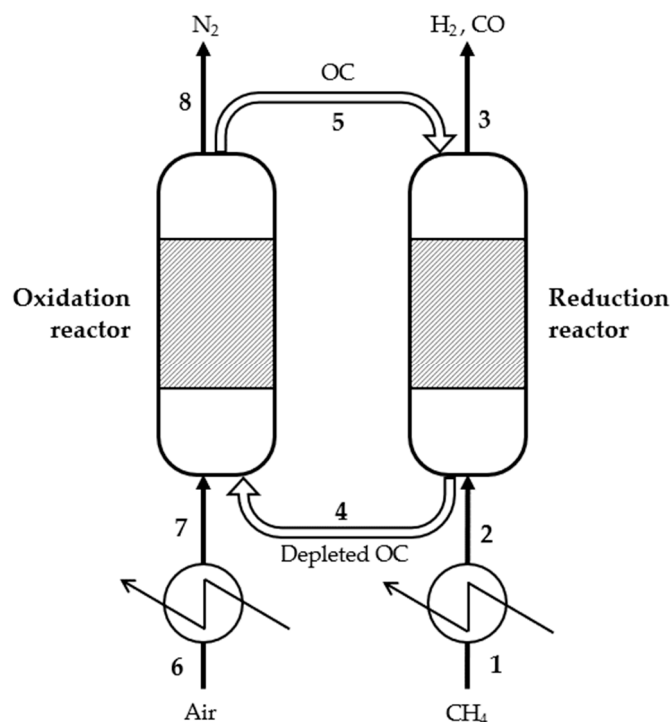
This approach does not account for kinetic or transport limitations, nor does it consider the chemical or mechanical degradation that the material may undergo during actual operation, meaning that the results presented here represent a theoretical limit. However, understanding this limit is valuable as it establishes a target, a maximum value that could potentially be achieved by optimizing certain operational parameters, and serves as a guide for identifying conditions that can enhance process performance.

2. Materials and Methods

2.1. Chemical-Looping Reforming Configuration

In order to analyze the reaction scheme, it is possible to represent the process as a set of two isothermal reactors (Scheme 1). Each of these reactors incorporates a preheating stage, which allows the gaseous feed streams (streams 1 and 6) to reach the specified reaction temperature before entering the reactor. In this configuration, the reduction reactor (or fuel reactor) is where the reaction between the oxygen carrier (stream 5) and CH_4 (stream 2) takes place. This step results in two streams: a gaseous stream where the primary products are H_2 and CO (stream 3) and a solid product stream containing the depleted

OC (stream 4). The second reaction step takes place in the oxidation reactor, where the depleted OC (stream 4) is regenerated from an oxidant (stream 7) which, in the case of this study, constitutes an air stream. The products of this reaction stage are divided into two streams: a solid stream consisting of the oxidized OC (stream 5), which is recirculated to the reduction reactor, and a gaseous stream (stream 8) consisting mainly of nitrogen.



Scheme 1. Chemical-looping reforming configuration. Stream 1: CH₄ (25 °C); stream 2: CH₄ (reduction temperature); stream 3: gaseous products from reduction reactor (reduction temperature); stream 4: depleted OC (reduction temperature); stream 5: regenerated OC (oxidation temperature); stream 6: air (25 °C); stream 7: air (oxidation temperature); stream 8: depleted air from oxidation reactor (oxidation temperature).

2.2. Chemical Equilibrium Model

In the first stage of the study, the equilibrium compositions obtained for the different OCs studied were determined by the total Gibbs free energy minimization method under different reaction conditions, specifically temperature and molar ratio of the reactants [32]. Assuming that equilibrium is reached in each reactor, the non-stoichiometric method of total Gibbs free energy minimization allows the determination of the compositions of the exit streams, without defining specific reactions.

This approach is based on the premise that a system subjected to constant pressure and temperature will decrease its total Gibbs free energy to a minimum value until it reaches equilibrium. In a system comprising N species, the total Gibbs free energy can be calculated by Equation (1). In this expression, n_i represents the number of moles of the i -th species, and \bar{g}_i the respective partial Gibbs free energy, which can be calculated considering the Gibbs free energy in the normal state (g_i°) and the activity (a_i).

$$G = \sum_i^N n_i \bar{g}_i = \sum_i^N n_i (g_i^\circ + RT \ln a_i) \quad (1)$$

Assuming ideal gas behavior and setting the pressure at 1 atm, the activity of gaseous species can be represented by their mole fraction. For solid species, unit activity is considered since they exist as pure phases without forming solid solutions. Additionally, the

Gibbs free energy of a pure compound in its normal state (g_i°) is equal to its standard Gibbs free energy of formation ($\Delta g_{f_i}^\circ$), which represents the energy change when the compound is formed from its elements, whose reference Gibbs free energy is zero. With these simplifications, Equation (1) can be reduced to Equation (2), where N_{gas} represents the number of species present in the gas phase, and N_{sol} refers to those in the solid phase, while n_{gas} indicates the total number of moles that constitute the gas phase.

$$G = \sum_i^{N_{\text{gas}}} n_i \left[\Delta g_{f_i}^\circ + \left(\frac{n_i}{n_{\text{gas}}} \right) \right] + \sum_i^{N_{\text{sol}}} n_i \Delta g_{f_i}^\circ \quad (2)$$

Thus, to determine the equilibrium compositions, the number of moles n_i must minimize the function given by Equation (2), while satisfying the mass balance constraints outlined in Equation (3) for the K chemical elements present in the system. In this equation, $\alpha_{i,k}$ stands for the number of atoms of the k -th element in the molecule of the i -th species. This implies that the number of moles of each atomic element must remain constant in the system, with a value equal to A_k .

$$\sum_i^N n_i \alpha_{i,k} = A_k \quad (3)$$

The Gibbs free energy of formation of each species at the reaction temperature (Δg_{f_i}) needed for Equation (2) were calculated by Equation (4). The enthalpy (Δh_{f_i}) and the entropy (Δs_{f_i}) of formation were calculated by Equations (5) and (6). Also, Equation (7) defines Δcp , where v_i represents the stoichiometric coefficient of each species associated with its formation reaction, while $cp_i(T)$ stands for the heat capacity of the compound at the reaction temperature. The standard state formation properties ($\Delta h_{f_i}^s$ and $\Delta s_{f_i}^s$) and $cp_i(T)$ expressions used in these equations were obtained from references [33–36] or by calculation using the inorganic solid prediction method developed by Mostafa et al. [37,38]. In this study, all species were modeled based on their unique thermodynamic properties, which were obtained from reliable databases to ensure accurate representation of their behavior. Tables S1 and S2 in the Supplementary information summarizes the formation properties in the standard state and the coefficients for $cp_i(T)$ utilized in Equations (4)–(7).

$$\Delta g_{f_i}(T) = \Delta h_{f_i}(T) - T \Delta s_{f_i}(T) \quad (4)$$

$$\Delta h_{f_i}(T) = \Delta h_{f_i}^s + \int_{T^s}^T \Delta cp \, dT \quad (5)$$

$$\Delta s_{f_i}(T) = \Delta s_{f_i}^s + \int_{T^s}^T \frac{\Delta cp}{T} \, dT \quad (6)$$

$$\Delta cp = \sum_i v_i cp_i(T) = \sum_i v_i \left(a_i + b_i T + c_i T^2 + d_i T^3 + \frac{e_i}{T^2} \right) \quad (7)$$

In order to solve the minimization problems, it is first necessary to define the chemical species that may be present in the system, including both the reactants and any potential reaction products. For the gas phase, the species considered were the same for all the OCs. In the case of the fuel reactor where the syngas production takes place, the species considered were CH_4 , H_2 , CO , CO_2 , and H_2O , while for the regeneration step, the species defined were O_2 and N_2 . On the other hand, the solid species considered, which are determined by the nature of the analyzed OC, are detailed in Table 1. These species were selected based on previous literature reports regarding the reduction or oxidation reactions of W , Mn , and Ni [39–44]. The formation of WC or W_2C was not considered, as the reaction

conditions required for their formation, according to the literature [45,46], are not met in the present study.

Table 1. Solid species considered for the equilibrium calculation for each oxygen carrier.

Oxygen Carrier	Reduction	Oxidation
WO ₃	WO ₃ /WO ₂ /W, C	W/WO ₂ /WO ₃
MnWO ₄	MnWO ₄ , WO ₃ /WO ₂ /W, MnO ₂ /Mn ₂ O ₃ /Mn ₃ O ₄ /MnO/Mn, C	MnWO ₄ , W/WO ₂ /WO ₃ , Mn/MnO/Mn ₃ O ₄ /Mn ₂ O ₃ /MnO ₂
NiWO ₄	NiWO ₄ , WO ₃ /WO ₂ /W, NiO/Ni, C	NiWO ₄ , W/WO ₂ /WO ₃ , Ni/NiO

Some authors have expressed concerns regarding the potential sublimation of WO₃ at temperatures around 800 °C, which may limit its applicability. However, Millner and Neugebauer reported that tungsten oxides do not sublime at an appreciable rate below 1000 °C, either in vacuum or in a stream of neutral gas [47]. These findings are consistent with the vapor pressure data for WO₃ reported by Blackburn et al. [48], who experimentally determined that at 1041 °C, the vapor pressure of WO₃ is 9.67×10^{-7} atm. Additionally, recent thermogravimetric analysis conducted by J. Wendel showed no evidence of WO₃ sublimation below 1100 °C in either dry helium or air [49]. This clearly demonstrates that sublimation would not occur under the reaction conditions studied in this work and thus only WO₃ in solid state was considered.

According to the results obtained from the total Gibbs free energy minimization for each OC, considering all the species detailed in Table 1, only some of them were identified across the range of temperatures and reactant ratios analyzed. In the gas phase, the observed species were CH₄, H₂, CO, H₂O, and CO₂. In the solid phase, the species identified for each OC were as follows:

WO₃: W, WO₂, WO₃, C;

MnWO₄: W, MnO, MnWO₄, C;

NiWO₄: W, WO₂, Ni, NiWO₄, C.

Considering this, the reactions between CH₄ and the OCs to produce H₂ and CO as gas products, along with the most reduced species of the oxygen carriers identified in the equilibrium calculations, were defined. This led to Equations (8)–(10), where the stoichiometry was defined such that 1 mol of the OC is reduced in all cases.



It is important to clarify that these are not the only reactions occurring in the reduction reactor. Depending on the reaction conditions, other reactions may include the thermal decomposition of CH₄, carbon gasification, CH₄ reforming with H₂O or CO₂, the water–gas shift reaction, total oxidation of CH₄ by the OCs, and partial reduction of the OC, among others. However, the reactions defined by Equations (8)–(10) govern the system, as the goal of this stage is syngas production through the reduction of metal oxides.

The reaction temperature varied between 500 and 1000 °C independently for each reactor. To analyze the effect of the reactant ratio, the initial amount of CH₄ in stream 1 was fixed based on the quantity required to reduce one mole of each OC, according to Equations (8)–(10). These reactions define the stoichiometric ratios CH₄: OC, which were 3:1 for WO₃ and MnWO₄, and 4:1 for NiWO₄. Consequently, the number of moles of CH₄ in stream 1 was maintained at a constant value of 3 for WO₃ and MnWO₄, and 4 for NiWO₄,

while the amount of the OCs' moles (stream 5) varied by $\pm 25\%$ and $\pm 50\%$ relative to the stoichiometric value of 1. Specifically, the OC quantities analyzed were 0.50, 0.75, 1.0, 1.25, and 1.50 moles.

Accordingly, after reaching equilibrium, the compositions at the reactor outlet (streams 3 and 4) were obtained for all the temperatures and reactant ratios analyzed for each OC. The conversions of the OCs and CH_4 , along with the yields towards H_2 and C, were then calculated based on Equations (11)–(14). In these equations, Y_i stands for the yield towards the i -th product, n_i^{eq} denotes the moles of the i -th species at equilibrium, and n_i° refers to the initial amount of i -th species.

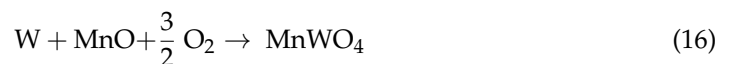
$$\text{OC conversion} = \frac{(n_{\text{OC}}^{\circ} - n_{\text{OC}}^{\text{eq}})}{n_{\text{OC}}^{\circ}} \cdot 100\% \quad (11)$$

$$\text{CH}_4 \text{ conversion} = \frac{(n_{\text{CH}_4}^{\circ} - n_{\text{CH}_4}^{\text{eq}})}{n_{\text{CH}_4}^{\circ}} \cdot 100\% \quad (12)$$

$$Y_{\text{H}_2} = \frac{n_{\text{H}_2}^{\text{eq}}}{2 \cdot n_{\text{CH}_4}^{\circ}} \cdot 100\% \quad (13)$$

$$Y_{\text{C}} = \frac{n_{\text{C}}^{\text{eq}}}{n_{\text{CH}_4}^{\circ}} \cdot 100\% \quad (14)$$

Based on the results of this stage, the conditions that did not lead to carbon formation, according to Equation (14), were selected for the subsequent oxidation of the depleted OC in the regeneration reactor. The re-oxidation was carried out by an air stream and the effect of the reaction temperature and reactant ratio was also studied for this stage. As in the fuel reactor, the equilibrium compositions were calculated considering all the species presented in Table 1 for the solid phases. After that, the reactions that lead to the oxidation of the reduced species of the OCs with O_2 were defined (Equations (15)–(17)).



Accordingly, the amount of the oxidizing agent was modified by $\pm 10\%$, $\pm 20\%$, and $\pm 30\%$ with respect to the stoichiometry determined by Equations (15)–(17). From this stage, only those conditions that led to complete regeneration of the OCs were selected for the energy analysis. Subsequently, to gain a deeper understanding of the influence of the reaction conditions, their effects on the system's energy requirements were analyzed and compared.

2.3. Energy Balances

For the purpose of this analysis, it has been assumed that the gaseous CH_4 and air feed streams are provided at a temperature of $25\text{ }^{\circ}\text{C}$. As mentioned above, the introduction of a preheating stage upstream of each reactor allows the streams to reach the required reaction temperature, which is also the temperature of the effluent streams. Therefore, for the reduction stage, $T_{\text{red}} = T_2 = T_3 = T_4$, while for the oxidation stage, $T_{\text{ox}} = T_7 = T_8 = T_5$.

Since each reactor operates isothermally, heat must be added or removed to maintain the reaction at a constant temperature. The total heat of reaction of a system (Q_{R}) can be attributed to the contributions of all the reactions taking place in it. To calculate the heat of

reaction of either the fuel or regeneration reactor, it is necessary to consider the respective enthalpy of each reaction (ΔH_r) in addition to its extent of reaction (X_r), as expressed by Equation (18).

$$Q_R = \sum_r^R X_r \Delta H_r \quad (18)$$

In the case of the fuel reactor, since the main reactions taking place are endothermic, heat should be added to operate isothermally ($Q_R > 0$). On the other hand, the oxidation of the depleted oxygen carrier that takes place in the regeneration reactor is exothermic, so heat should be removed ($Q_R < 0$). In the Supplementary Materials, Figure S1 shows the variation of ΔH_r as a function of temperature for the main reactions occurring in the systems studied (Equations (8)–(10) and (15)–(17)).

Alternatively, considering that the composition of the inlet and outlet streams was determined by the previous equilibrium calculations, the heat flows can be calculated by applying the energy balances to each reactor (Equation (19)).

$$Q = H_{\text{outlet}} - H_{\text{inlet}} \quad (19)$$

In particular, for the system under consideration, the energy balances for each reactor can be expressed by Equations (20) and (21), where Q_{red} represents the heat that must be supplied in the fuel reactor and Q_{ox} the heat that must be extracted from the oxidation reactor to achieve isothermal operation.

$$Q_{\text{red}} = H_3 + H_4 - (H_2 + H_5) \quad (20)$$

$$Q_{\text{ox}} = H_8 + H_5 - (H_7 + H_4) \quad (21)$$

In addition, the heat flows required for the preheating stages to bring the gas streams up to the required temperatures for the reduction and oxidation reactors, $Q_{\text{p}_{\text{red}}}$ and $Q_{\text{p}_{\text{ox}}}$, respectively, can be calculated by Equations (22) and (23).

$$Q_{\text{p}_{\text{red}}} = H_2 - H_1 \quad (22)$$

$$Q_{\text{p}_{\text{ox}}} = H_7 - H_6 \quad (23)$$

The enthalpy of each stream (j) depends on its composition and temperature, and it can be expressed by Equation (24). In this expression, the enthalpy of each species can be calculated by Equation (25), where the reference has been established as pure compound at 25 °C and 1 atm.

$$H_j = \sum_i n_i h_i(T) \quad (24)$$

$$h_i(T) = \Delta h_{f,i}^s + \int_{T^s}^T c_{p,i} dT \quad (25)$$

In summary, the energy balance for the whole system can be expressed by Equation (26), where Q_{CLR} represents the net heat of the chemical-looping reforming process.

$$Q_{\text{CLR}} = Q_{\text{red}} + Q_{\text{ox}} + Q_{\text{p}_{\text{red}}} + Q_{\text{p}_{\text{ox}}} \quad (26)$$

In this context, to avoid external energy input, Q_{CLR} must be zero or negative. During the process, energy is consumed in the preheating stages and by the endothermic reactions occurring in the reduction reactor. To satisfy the heat balance without the need for any external energy source, the heat generated in the regeneration reactor must be sufficiently high. Therefore, Equation (27) must be fulfilled.

$$|Q_{\text{ox}}| > Q_{\text{red}} + Q_{\text{p}_{\text{red}}} + Q_{\text{p}_{\text{ox}}} \quad (27)$$

In order to determine the reaction conditions that allow the system to operate without the need for external energy input, each heat flow was determined from Equations (20)–(27) and the effect on Q_{CLR} was then analyzed.

3. Results and Discussion

3.1. Chemical Equilibrium

3.1.1. Reduction Reactor

As a result of the minimization of the total Gibbs free energy (Equations (1)–(3)), the product distribution corresponding to the composition of streams 3 and 4 was obtained for the different OCs (Figures S2–S4 of the Supplementary Materials).

In terms of solid conversion defined by Equation (11), Figure 1a–c reveal evident differences between the OCs studied. Complete conversion of WO_3 was achieved over the whole range of temperatures and reagent ratios studied in contrast to the mixed oxides $MnWO_4$ and $NiWO_4$ where conversion values increase as temperature rises. It is observed that, at a fixed temperature, the conversion of WO_3 is greater than that of $NiWO_4$, with $MnWO_4$ showing the lowest conversion. This trend corresponds with the sequence of the ΔG_r values of the reactions defined by Equations (8)–(10), as illustrated in Figure S5 of the Supplementary Materials, where the reduction of WO_3 exhibits the most negative value. For instance, at 600 °C and stoichiometric ratios $CH_4:OC$, $MnWO_4$ exhibits a conversion of only 3%, while $NiWO_4$ achieves 50%, and WO_3 reaches 100%. Furthermore, to obtain complete conversion, for $MnWO_4$ reaction, temperatures must exceed 775 °C, whereas for $NiWO_4$, complete conversion occurs at 700 °C.

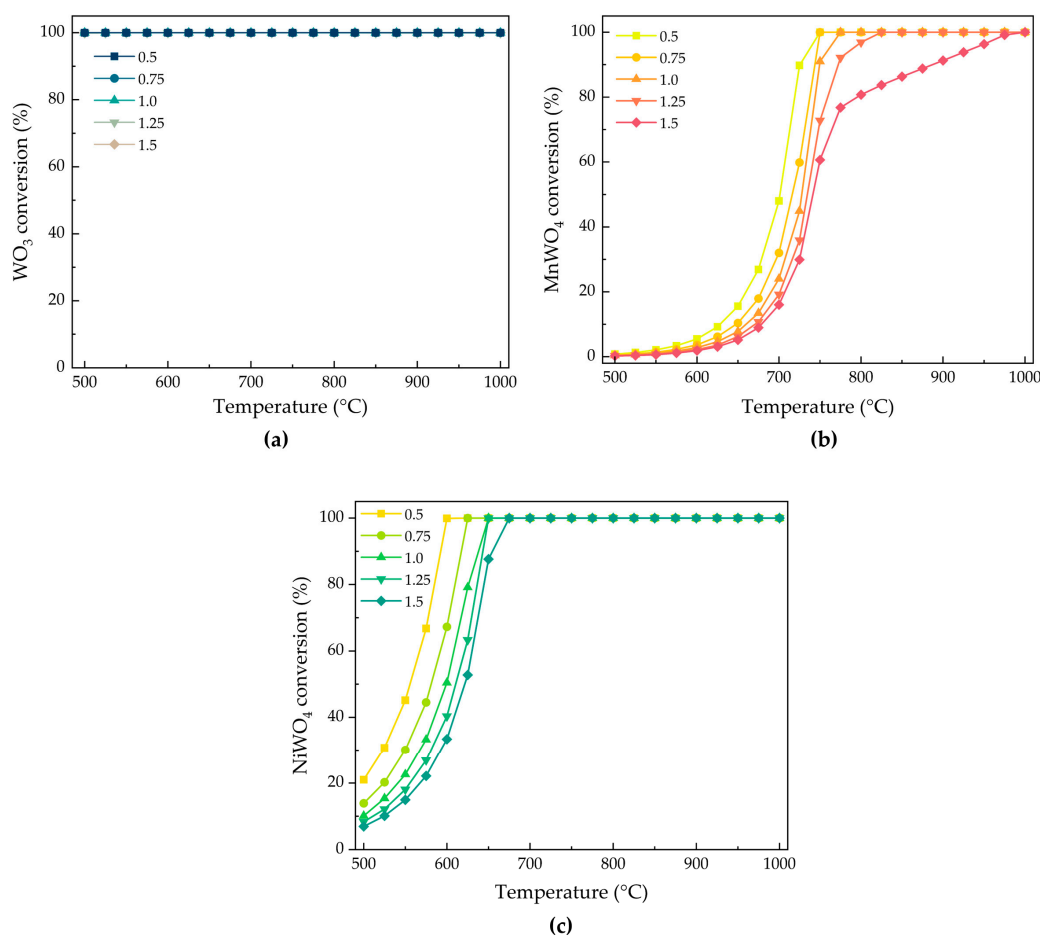


Figure 1. Conversion of the oxygen carrier as a function of reduction temperature, parameterized for different mole amounts of (a) WO_3 ; (b) $MnWO_4$; (c) $NiWO_4$.

As expected, CH₄ conversion increases with temperature (illustrated in Figure S6a–c in the Supplementary Materials) due to the endothermic nature of the reactions in which it is involved as reactant, in accordance with the findings previously presented for several oxygen carriers [50,51]. Particularly, as observed by de Diego et al. for NiO [52], the conversion of CH₄ increases as the reaction temperature rises since it improves the reduction degree of the oxygen carrier, making more oxygen available for CH₄ oxidation, achieving conversion rates of up to 98% at 900 °C in a continuous experimental setup. In this work, maximum values were achieved at ratios above stoichiometric, allowing for complete conversion of CH₄ at temperatures of 825 °C for both WO₃ and NiWO₄, and at 875 °C for MnWO₄. These results seem to be in agreement with those reported by López-Ortiz et al. [53], who achieved complete CH₄ conversion at approximately 800 °C using CoWO₄ as the oxygen carrier with a molar ratio CH₄:OC = 4:1.5.

Figure 2a–c illustrate the selectivity towards the solid products for 1.5 moles of OC, but this trend is the same for the remaining CH₄:OC ratios. As shown in Figure 2a, for WO₃, the selectivity depends on the temperature, in agreement with the experimental results obtained by Kodama et al. [15]. At low temperatures, WO₂ is obtained as a solid product, indicating a partial reduction of the OC. Conversely, at higher temperatures, the only solid product is metallic W. In the case of MnWO₄, the selectivity towards the reduction products was found to be independent of temperature and CH₄:OC ratio, resulting in MnO and W (Figure 2b). This implies that only W undergoes a change in oxidation state from W⁺⁶ to W⁰, while Mn⁺² remains in its original state. These findings are in agreement with the products reported by Bustnes et al. [43] for the reduction of MnWO₄ by H₂. In contrast, the reduction of NiWO₄ results in Ni⁰ over the entire temperature range, while for W, the trend is analogous to the WO₃ case, where the complete reduction from W⁺⁶ to W⁰ occurs only at high temperatures. Sridhar et al. [42] also studied the reduction of NiWO₄ by H₂ and reported that the reaction proceeds in two steps: first, reduction of NiWO₄ to Ni and WO₂, followed by a second step where WO₂ is further reduced to metallic tungsten, which is consistent with the results obtained in this study.

With regard to carbon formation, Figure 3a–c show the carbon yield, defined by Equation (14), as a function of the reduction temperature and the number of moles of OC. It can be observed for all cases, that carbon formation is significant for most of the conditions studied, especially when there is insufficient OC and at low temperatures.

A maximum in carbon yield is observed at temperatures between 600–700 °C, reaching maximum values of 58% for WO₃, 68% for MnWO₄, and 55% for NiWO₄, each associated with CH₄ conversions of 65%, 76%, and 63%, respectively (Figure S6a–c). Lower temperatures facilitate the formation of carbon, as the reaction of CH₄ undergoing thermal decomposition to produce C and H₂ has a lower value of ΔG_r than the other reactions, as observed in Figure S5 in the Supplementary Materials. So, the maximum in carbon yield can be linked to the increase in CH₄ conversion within the temperature range where the reduction reactions of the OCs are not yet spontaneous. At higher temperatures, as these reactions shift their ΔG_r to negative values, the carbon yield decreases as the temperature rises. These results are in agreement with the existing literature. For example, Jerndal et al. [54] studied various oxygen carriers by simulating reactions and found that lower temperatures and smaller amounts of added oxygen promote carbon formation. Additionally, at low temperatures, more oxygen is required to prevent carbon deposition, whereas at higher temperatures, less oxygen is needed. Thermodynamic calculations on carbon deposition using tungsten oxides as oxygen carriers were also conducted by Kang et al. [55], indicating that significant carbon deposition does not occur if the sufficient oxygen is provided by the metal oxide. Moreover, Cho et al. [56] performed the reaction in a laboratory fluidized-bed reactor with oxygen carriers containing nickel

and found that when sufficient oxygen in the oxide was still available, there was limited formation of carbon independent of temperature in the investigated range of 750–950 °C, but when more than 80% of the available oxygen was consumed, rapid formation of carbon was observed. Thus, carbon formation happens when fuel oxidation cannot take place substantially.

For sub-stoichiometric ratios, significant carbon formation is observed throughout the whole temperature range. Conversely, Table 2 displays the temperature values above which carbon yield is zero (0.0%) for stoichiometric and excess of OC conditions.

The stoichiometric ratios result in the highest temperature limits for WO_3 and NiWO_4 . Regarding MnWO_4 , carbon formation is observed even at temperatures up to 1000 °C. It is noted that the region with no carbon formation corresponds to elevated OC conversion and to the zone where the solid products are the most reduced species of each OC, i.e., W in the case of WO_3 , MnO and W for MnWO_4 , and finally Ni and W for NiWO_4 .

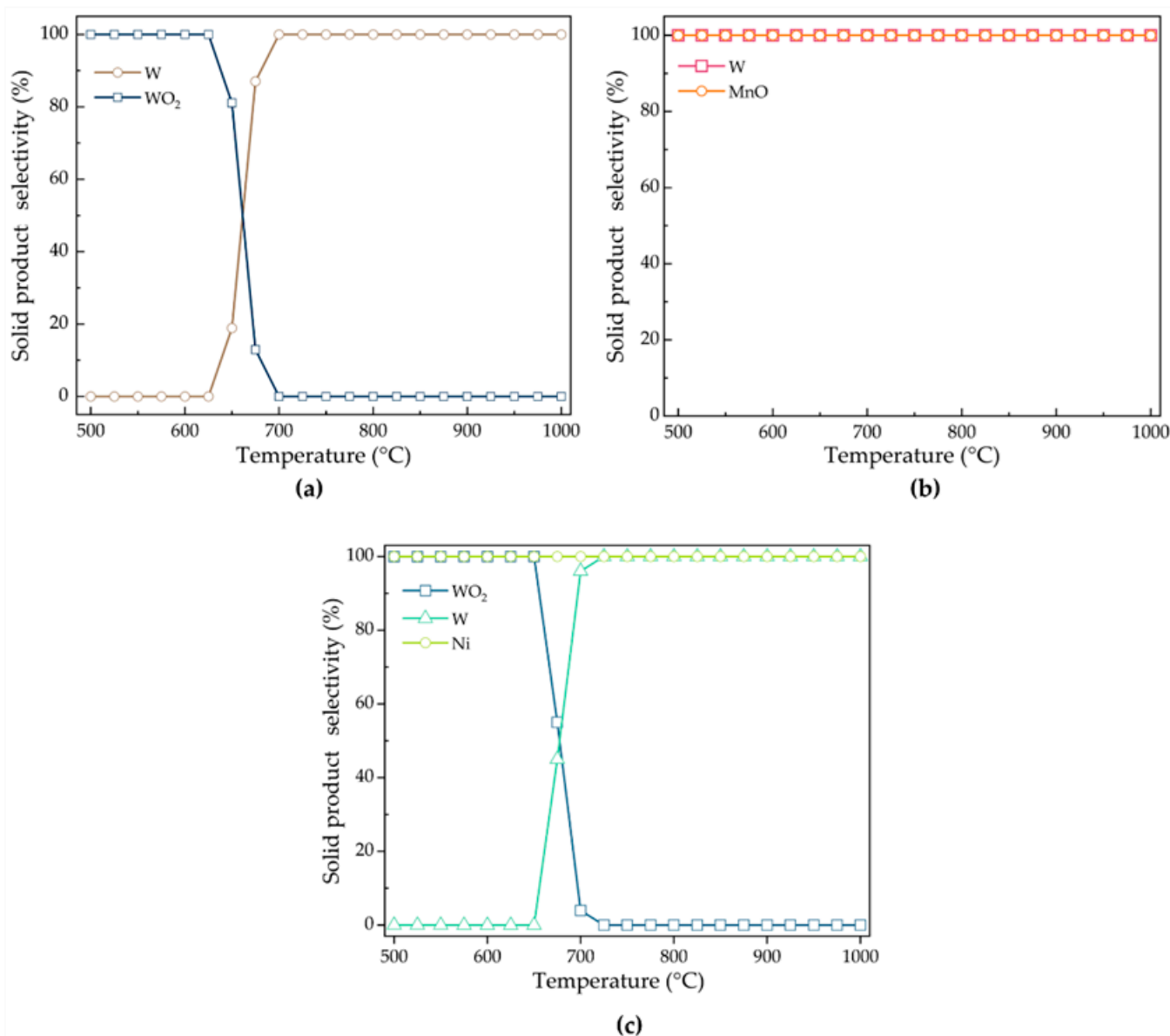


Figure 2. Selectivity towards solid products as a function of reduction temperature for 1.5 moles of (a) WO_3 ; (b) MnWO_4 ; (c) NiWO_4 .

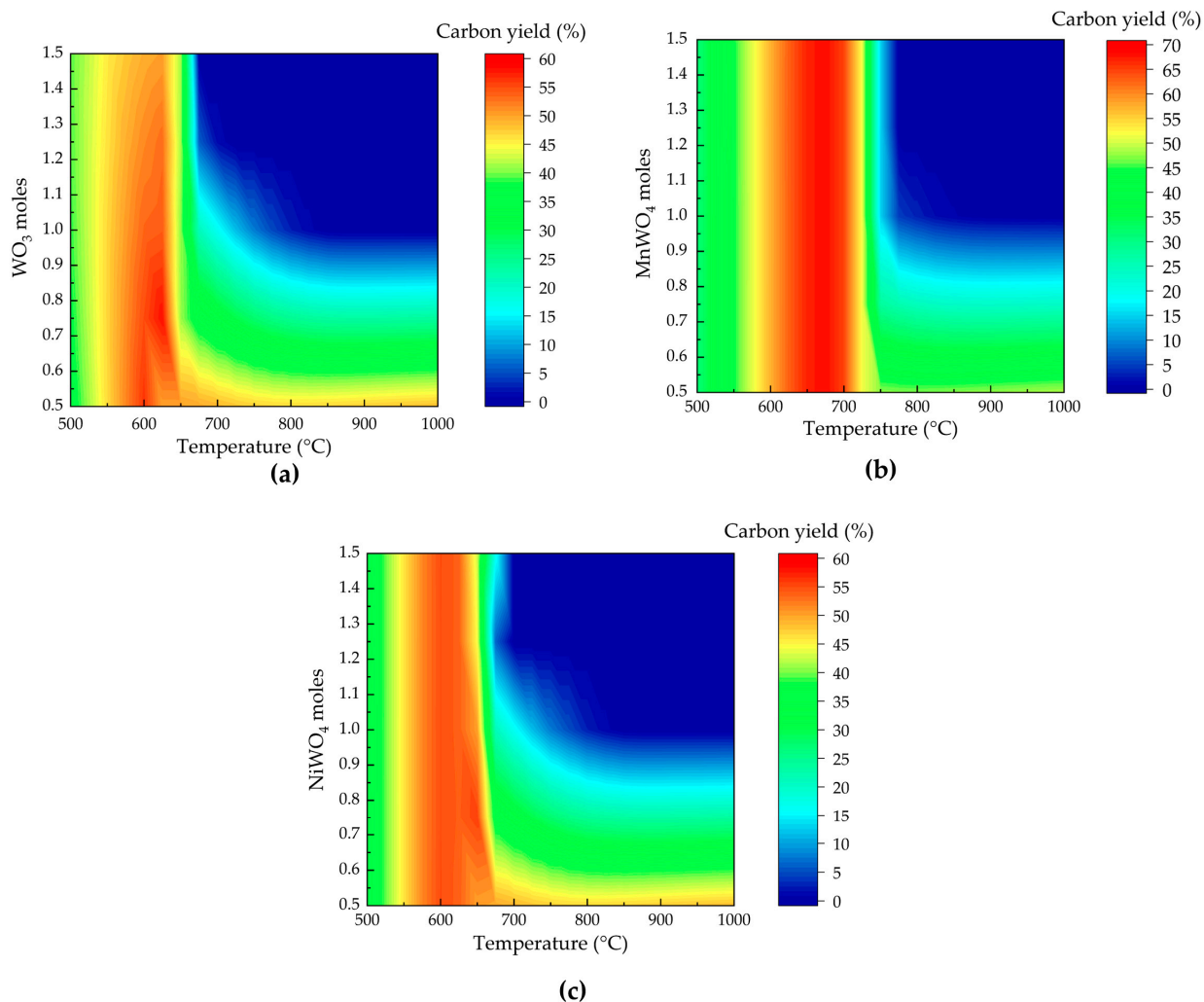


Figure 3. Carbon yield as a function of reduction temperature and mole amounts of (a) WO_3 ; (b) MnWO_4 ; (c) NiWO_4 .

Table 2. Temperature values above which the carbon yield is zero.

OC Moles	WO_3	MnWO_4	NiWO_4
1.0	875 °C	*	875 °C
1.25	725 °C	775 °C	700 °C
1.5	700 °C	775 °C	700 °C

* Carbon is observed across the entire temperature range analyzed.

A correlation between OC conversion, selectivity towards different solid products, and carbon formation can be made. As the conversion of the OC increases (along with the increase in selectivity towards the most reduced species, as shown in Figure 2a,c), the amount of carbon formed decreases. This is because the oxygen present in the OC now becomes part of the oxidation products, mainly producing CO. Furthermore, as the amount of OC available increases, the formation of CO_2 due to total oxidation reactions is also observed. Therefore, high temperatures and a higher amount of OC moles imply a lower carbon yield (zone indicated with blue color in Figure 3a–c).

Regarding the H_2 yield shown in Figure 4a–c, a similar trend is observed for all the OCs, with the highest values obtained for 0.5, 0.75, and 1 moles of OC.

In these cases, the H_2 yield increases with temperature over the whole range, whereas when considering 1.25 or 1.5 moles of OC, the H_2 yield presents a maximum value from which it remains approximately constant or decreases with further increase in temperature.

This is attributed to the formation of total oxidation products (H_2O and CO_2), arising from the increased availability of oxygen from the more reduced species of the oxygen carriers, which leads to a decrease in selectivity towards H_2 . Several authors have reported this behavior through both theoretical and experimental studies, noting higher yields of H_2 under stoichiometric ratios. For instance, de Diego et al. [52] achieved a maximum H_2 yield of 90% when using NiO as the OC with a $CH_4:OC$ ratio of 1:1 in a continuous reactor, while Yahom et al. [57] reached equivalent conclusions by simulation, employing the same OC.

It is verified that the stoichiometric ratios between the reactants enable the achievement of maximum H_2 yields, and under these conditions, this is favored by the high reaction temperatures, obtaining a maximum value of 98% at 1000 °C for all the OCs, while at the same temperature, with 1.5 moles of OC, for example, the yield decreases to 81%.

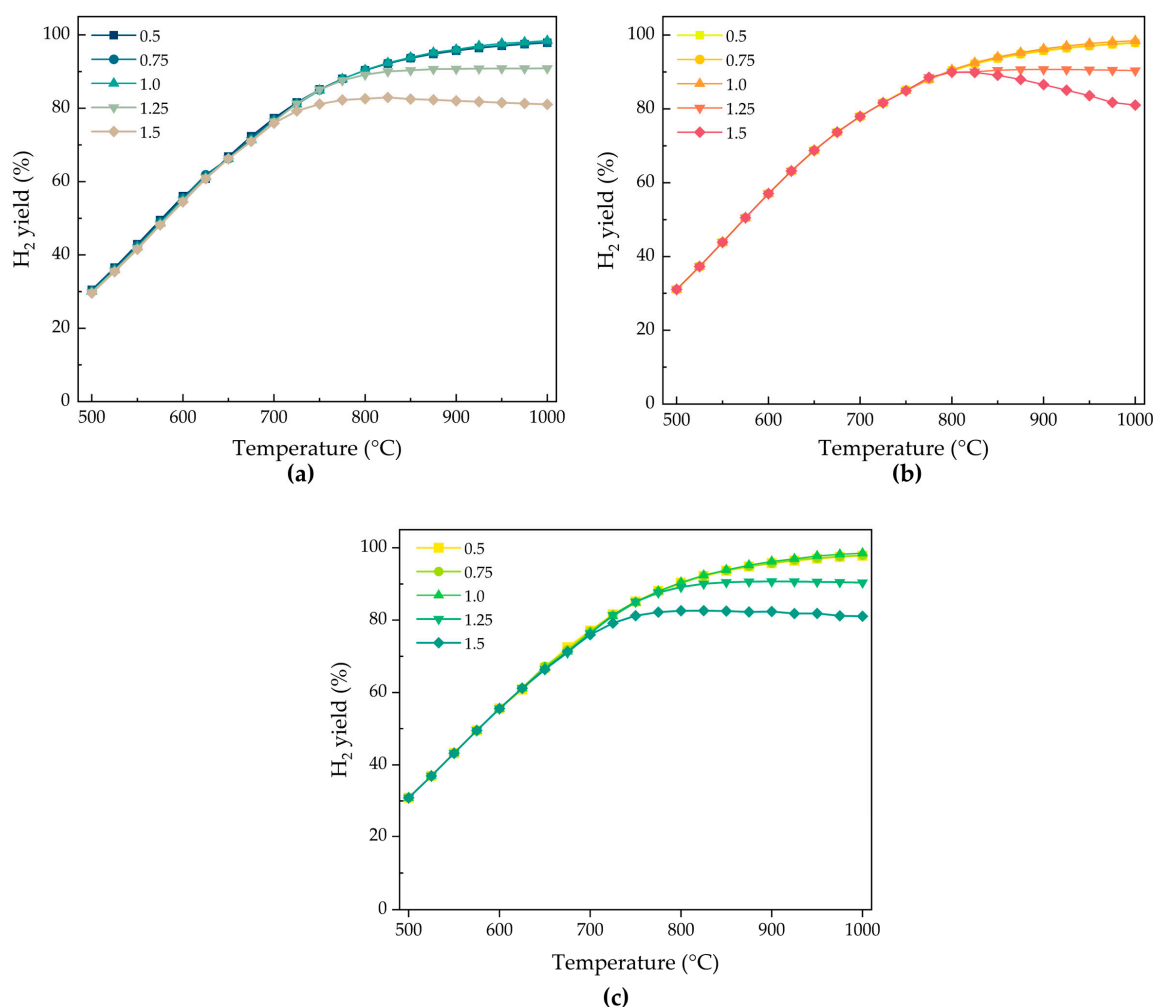


Figure 4. H_2 yield as a function of reduction temperature, parameterized for different mole amounts of (a) WO_3 ; (b) $MnWO_4$; (c) $NiWO_4$.

3.1.2. Oxidation Reactor

With regard to the regeneration stage, equilibrium calculations were carried out for the different compositions previously obtained for stream 4, under conditions where carbon formation is avoided. This is crucial to prevent solid deactivation and CO_2 production in the regeneration reactor as a result of gasification reactions with the oxidants [50]. The compositions obtained are presented in Figure S7a–c in the Supplementary Materials.

As mentioned above, these conditions coincide with those in which the species W, MnO, and/or Ni are obtained as solid products. In addition, in the case of $MnWO_4$, stream

4 may contain unreduced OC, since its conversion may be less than 100%, while for NiWO_4 and WO_3 , the conditions that do not generate carbon coincide with those in which there is complete conversion. It was found that the percentage of OC regenerated and the product distribution obtained were independent of temperature, possibly due to the highly negative ΔG_r value determined for reactions defined by Equations (15)–(17), as observed in Figure S5 in the Supplementary Materials.

Figure 5a–c illustrate the product distribution obtained by regenerating the depleted OCs (that is, W for WO_3 , W and MnO for MnWO_4 , and W and Ni for NiWO_4) with different amounts of air. In the x-axis, the value 0% represents the stoichiometric ratio between O_2 and the OC according to the reactions defined by Equations (15)–(17), while the percentages ± 10 , ± 20 , $\pm 30\%$ indicate the extent of the defect or excess considered for the oxidation reaction.

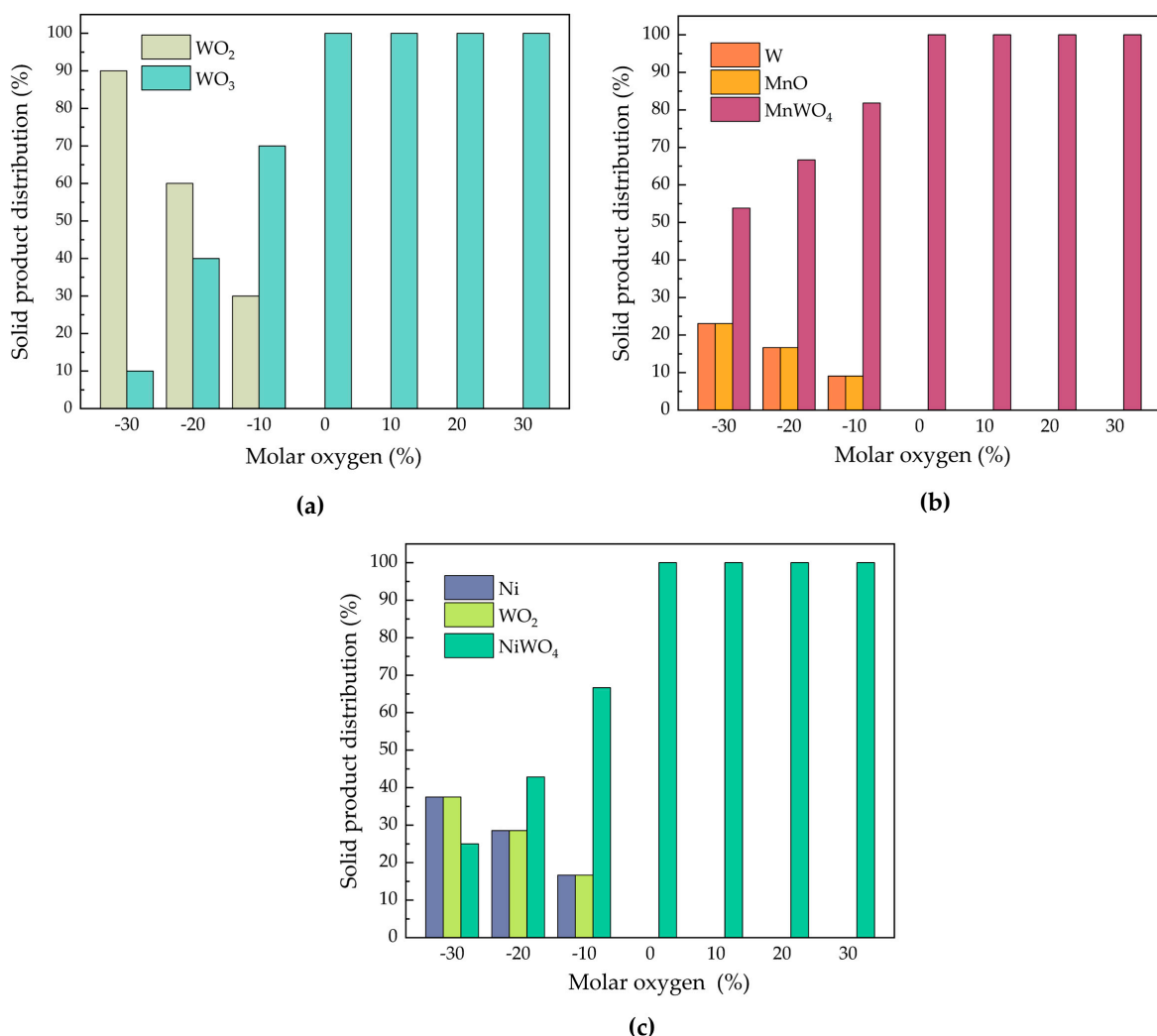


Figure 5. Solid product distribution for regeneration of the depleted OCs as a function of O_2 excess/defect for (a) WO_3 ; (b) MnWO_4 ; (c) NiWO_4 .

The results show that stoichiometric amounts of O_2 allowed the complete regeneration of the OCs. Conversely, under oxygen-deficient conditions, the percentage of regenerated oxide and the product distribution depended on the amount of O_2 used.

These results seem to align with those reported by various authors in the literature regarding the synthesis of these materials via solid-state reactions [58–65].

Considering that an excess of air during the preheating stage results in a higher heat demand and thus has a negative impact on the energy balance, it was determined that the amount of air used in the oxidation reactor should be stoichiometric, as this is the minimum required to achieve complete regeneration of the OCs.

3.2. Energy Balances

In addition to hydrogen yield, the energy balance of the process must be considered when assessing the performance of a given OC and the overall process. With this purpose, the results obtained for the composition of the streams were used to determine the heat involved in each stage of the process, as described by Equations (20)–(27), for the different combinations of CH₄:OC ratios and reaction temperatures, both reduction and oxidation. The heat requirements for the reduction reaction (Q_{red}) and the heat released by the regeneration reaction of each OC (Q_{ox}) were determined. In addition, the heat required to preheat the reactant streams from 25 °C to the appropriate reaction temperature was also determined ($Q_{\text{p,red}}$ and $Q_{\text{p,ox}}$).

3.2.1. Preheating Stages

For the preheating of the reduction reactor, $Q_{\text{p,red}}$ represents the heat required to bring CH₄ (stream 1) to the reduction temperature (T_{red}), while in the case of the regeneration reactor, $Q_{\text{p,ox}}$ denotes the heat required to bring air (stream 6) to the oxidation temperature (T_{ox}).

Table 3 summarizes the minimum and maximum values of the preheating heats found for each OC.

Table 3. Minimum and maximum preheating heats for each OC.

		WO ₃	MnWO ₄	NiWO ₄
Q _{p,red} (kJ)	Min	104	125	145
	Max	177	177	236
Q _{p,ox} (kJ)	Min	102	118	136
	Max	331	331	442

NiWO₄ demonstrates the highest values for $Q_{\text{p,red}}$ due to the fixed quantity of CH₄ set at 4 moles for this OC, in contrast to 3 moles for both WO₃ and MnWO₄. Given that the amount of CH₄ remains constant for each oxygen carrier, $Q_{\text{p,red}}$ is only dependent on the reaction temperature, so higher T_{red} values directly lead to an increased $Q_{\text{p,red}}$. This results in the maximum value for $Q_{\text{p,red}}$ at a reduction temperature of 1000 °C for all the OCs, while minimum values for $Q_{\text{p,red}}$ are obtained at the minimum reduction temperatures that were found for each OC, that is 700 °C for WO₃ and NiWO₄, and 775 °C for MnWO₄.

In contrast, $Q_{\text{p,ox}}$ depends on both the oxidation temperature T_{ox} and the amount of OC analyzed, since larger quantities of reduced OCs need an increased amount of O₂ for regeneration (along with the corresponding moles of N₂), thereby increasing $Q_{\text{p,ox}}$. For all the OCs, the maximum values for $Q_{\text{p,ox}}$ were obtained for an oxidation temperature of 1000 °C, while the minimum values correspond to 500 °C. As observed for $Q_{\text{p,red}}$, NiWO₄ also exhibits the highest $Q_{\text{p,ox}}$ values, as the regeneration of 1 mole of NiWO₄ requires 2 moles of O₂, while only 1.5 moles of O₂ are required for both WO₃ and MnWO₄. On the other hand, the minimum value of $Q_{\text{p,ox}}$ is obtained for the regeneration of 1 mol of WO₃ at an oxidation temperature of 500 °C.

3.2.2. Reduction Heat

From Equation (20), the heat required in the reduction stage was obtained for the different conditions of T_{red} , T_{ox} , and number of moles of OC, showing a similar trend for all the OCs analyzed, as illustrated in Figure 6a–c. As this stage is dominated by endothermic reactions, these are thermodynamically favored by increasing the reaction temperature (T_{red}), which implies a higher energy consumption and therefore an increase in the heat to be supplied. Conversely, an increase in the oxidation temperature reduces the external demand, as it results in a higher energy input from the OC to the reduction stage, given that it enters the reduction reactor at a higher temperature.

In general, as a result of increased conversion levels, a higher amount of OC directly correlates with a higher energy requirement, as shown in Figure 6a–c by the upper plane corresponding to the higher number of moles of OC. However, for MnWO_4 , this trend is reversed at low reduction temperatures and high oxidation temperatures (see the intersection of the surfaces in Figure 6b). This can be attributed to the fact that the energy input from the solid, originated from the high-temperature regeneration reactor, has a significant impact, coupled with the minor conversion levels of this oxygen carrier at 800 °C compared to WO_3 and NiWO_4 .

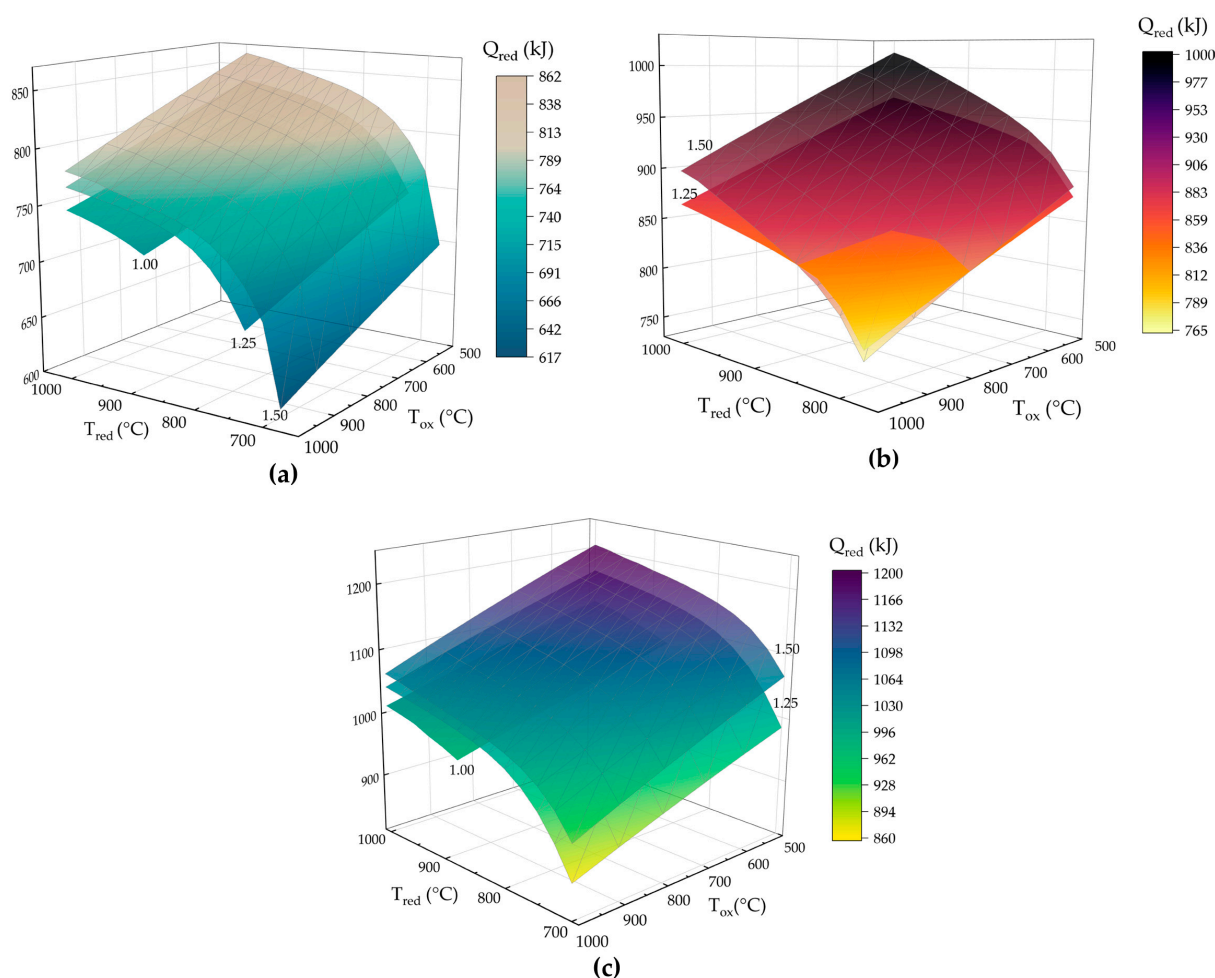


Figure 6. Heat required (Q_{red}) in the reduction reactor as a function of reduction and oxidation temperatures (T_{red} and T_{ox} , respectively), parameterized for different mole amounts of (a) WO_3 ; (b) MnWO_4 ; (c) NiWO_4 .

3.2.3. Regeneration Heat

From Equation (21), the heat generated in the regeneration stage by the exothermic reaction of oxidation of the depleted OC was determined. This heat is directly proportional to the amount of solid to be oxidized; therefore, larger amounts of OC result in higher Q_{ox} , as shown in Figure 7a–c for the different planes corresponding to 1, 1.25, and 1.5 moles of OC. Conversely, a slight decrease in Q_{ox} was observed for all OCs as the reaction temperature (T_{ox}) increased. This phenomenon can be attributed to a reduction in ΔH_f of the reactions defined by Equations (15)–(17) at higher temperatures, as illustrated in Figure S1 of the Supplementary Materials. For $MnWO_4$, it was observed that Q_{ox} is significantly influenced by the reduction temperature, as an increase in T_{red} leads to higher OC conversion at this stage. This results in a greater amount of reduced solid available for re-oxidation, ultimately leading to a higher Q_{ox} . This results in a crossover between the planes for 1.25 and 1.50 moles of $MnWO_4$ at high T_{ox} and low T_{red} , since part of the heat generated by the exothermic reaction is used to raise the temperature of the OC from T_{red} to T_{ox} , thereby reducing Q_{ox} . Conversely, the reduction temperature has a negligible effect on Q_{ox} for WO_3 and $NiWO_4$, as the conversion of both solids in the reduction reactor is complete within the temperature range analyzed.

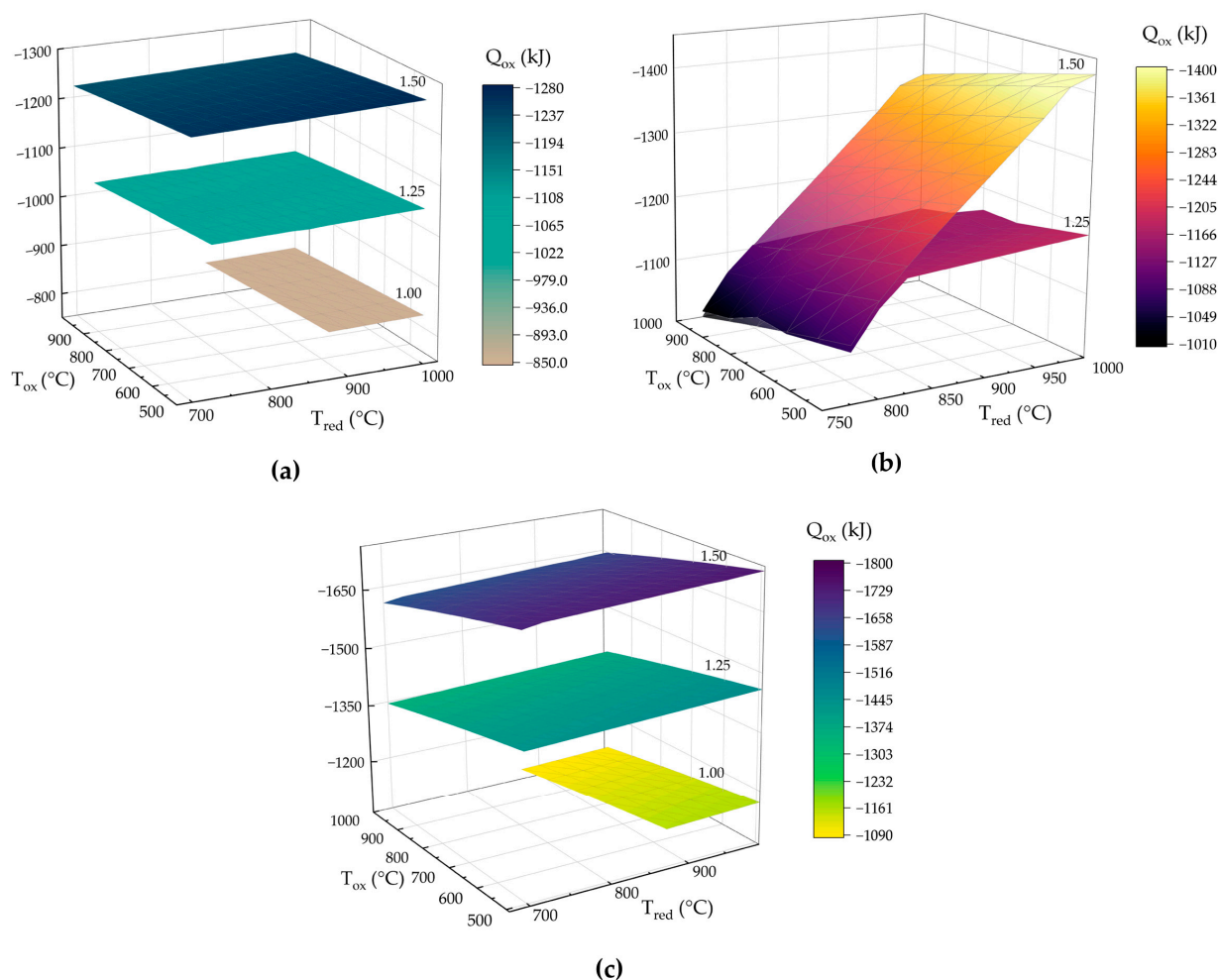


Figure 7. Heat released (Q_{ox}) in the oxidation reactor as a function of reduction and oxidation temperatures (T_{red} and T_{ox} , respectively), parameterized for different mole amounts of (a) WO_3 ; (b) $MnWO_4$; (c) $NiWO_4$.

3.2.4. Net Heat

From the calculations of Q_{red} , Q_{ox} , $Q_{\text{p,red}}$, and $Q_{\text{p,ox}}$, and taking into account the overall balance of the system, the net heat, named as Q_{CLR} , was determined by applying Equation (26). Figure 8a–c show Q_{CLR} as a function of the reduction and oxidation temperatures, with each plane corresponding to a specific number of moles of OC. In addition, a plane corresponding to $Q_{\text{CLR}} = 0$ (grey plane) has been included to enhance the visualization of the conditions that facilitate autothermicity. In this figure, positive Q_{CLR} values indicate that the heat generated in the oxidation reactor is insufficient to fulfill the heat balance (Equation (27) is not satisfied), needing external heat input. Conversely, more negative Q_{CLR} values mean a greater energy excess.

Regarding $\text{CH}_4:\text{OC}$ ratio, it is observed that higher amounts of OC have a positive effect on the system, as this results in greater energy transport by the solid from the oxidation reactor to the reduction reactor. This result aligns with those reported by other authors. For instance, Ortiz et al. [66] observed that when the oxygen supplied by NiO to the fuel reactor of a CLR system was at stoichiometric conditions for converting CH_4 to CO and H_2 , the process became energy demanding. They found that an excess of oxygen was necessary to achieve autothermal conditions, which in turn reduced the H_2 yield compared to stoichiometric conditions. Similarly, de Diego et al. [52] reported that for NiO, a molar ratio 25% above stoichiometric was necessary to satisfy the heat balance.

With respect to temperatures, in the case of WO_3 and NiWO_4 , negative values for Q_{CLR} are obtained for lower reaction temperatures for both oxidation and reduction reactors. Lower reaction temperatures result in less energy consumption for preheating the air and CH_4 streams. In addition, lower reduction temperatures require less energy for endothermic reactions due to the associated lower conversion. Finally, a lower oxidation temperature results in a greater release of heat during the regeneration reaction due to the more negative value of ΔH_r at lower temperatures. It can be noted that, regarding T_{ox} , although its rise significantly decreases the heat required for reduction (Q_{red} in Figure 6), the increase in the heat demand for preheating the air stream ($Q_{\text{p,ox}}$) has a greater impact in the overall energy balance, resulting in a detrimental effect. This can be observed in Figure 8, where an elevation in T_{ox} leads to a more positive value for Q_{CLR} .

On the other hand, the behavior of MnWO_4 differs from that of WO_3 and NiWO_4 , as its conversion depends on the reduction temperature, while WO_3 and NiWO_4 exhibit 100% solid conversion under the conditions analyzed in the energy balance. Upon reaching full OC conversion, which occurs at temperatures above $975\text{ }^\circ\text{C}$ and $850\text{ }^\circ\text{C}$ for 1.5 and 1.25 moles of MnWO_4 , respectively, the effect of T_{ox} and T_{red} becomes analogous to those observed for WO_3 and NiWO_4 . However, at lower temperatures, the trend is reversed, resulting in an improved energy balance with increasing T_{red} . Although an increase in the reduction temperature implies an increase in $Q_{\text{p,red}}$ and Q_{red} due to the higher conversion, as well as $Q_{\text{p,ox}}$ due to the greater amount of oxygen required to regenerate the depleted OC, the effect on the overall energy balance is compensated by an increase in the heat released during the oxidation of the depleted OC, Q_{ox} . As shown in Figure 7a,c, the effect of the reduction temperature on Q_{ox} is negligible for WO_3 and NiWO_4 as these OCs are fully converted. Therefore, in order to optimize the energy performance of MnWO_4 , it is essential that the solid undergoes the highest possible degree of conversion.

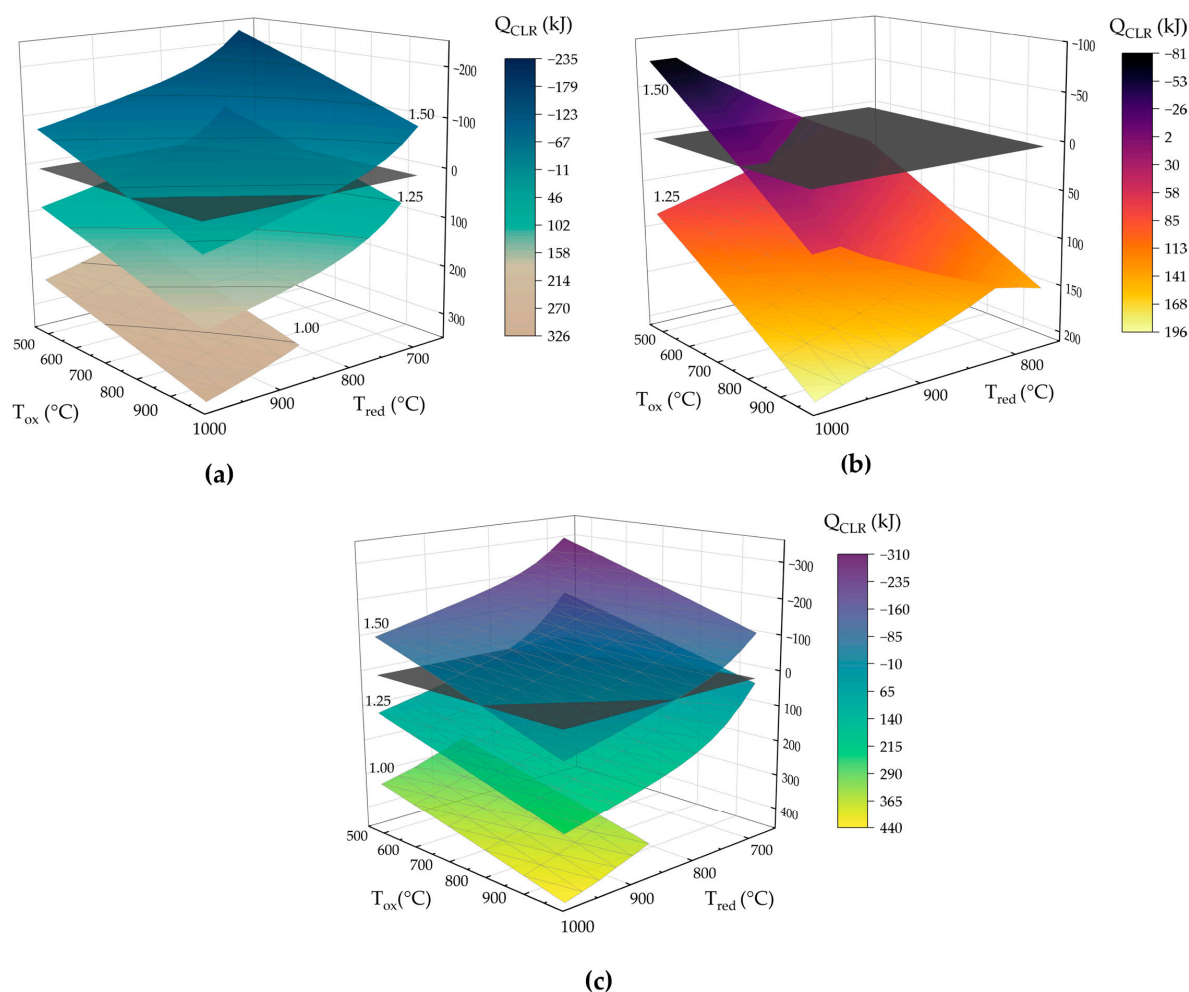


Figure 8. Net heat (Q_{CLR}) as a function of reduction and oxidation temperatures (T_{red} and T_{ox} , respectively), parameterized for different mole amounts of (a) WO_3 ; (b) $MnWO_4$; (c) $NiWO_4$.

Considering these factors, the conditions under which the system exhibits autothermicity were identified for each OC. It was determined that autothermicity is not achievable for WO_3 and $NiWO_4$ at stoichiometric ratios, but can be reached with 1.25 and 1.5 moles of OC. For $MnWO_4$, autothermicity is only feasible when considering 1.5 moles of the OC.

For 1.5 moles of WO_3 , if the reduction temperature is maintained below 825 °C, the process is autothermal across the entire range of oxidation temperatures. However, for 1.25 moles, both the reduction and oxidation temperatures must be kept below 800 °C. In the case of $NiWO_4$, the same trend as WO_3 is observed for 1.5 moles, while for 1.25 moles, autothermal operation can be achieved at reduction temperatures below 775 °C, accompanied by lower oxidation temperatures. In the case of $MnWO_4$, the reduction temperature must exceed 850 °C, while the oxidation temperature should remain below 800 °C.

3.3. H_2 Yield vs. Autothermal Conditions

As observed from the previous analysis, the temperature ranges that lead to autothermal operation are broader for WO_3 and $NiWO_4$, whereas for $MnWO_4$, this range is more limited. Table 4 presents the maximum H_2 yield obtained under autothermal conditions, along with the corresponding reduction temperature and CH_4 :OC ratio. Additional parameters, such as CH_4 conversion, are also included. Based on these reduction conditions, the maximum net heat is shown, along with the corresponding oxidation temperature.

Table 4. Conditions that maximize H₂ yield under autothermal operation.

	WO ₃	MnWO ₄	NiWO ₄
H ₂ yield (%)	88	88	88
T _{red} (°C)	775	875	775
CH ₄ :OC ratio	3:1.25	3:1.50	4:1.25
H ₂ :OC relation	4.208	3.52	5.608
CH ₄ conversion (%)	97	100	97
T _{ox} (°C)	500	500	500
Q _{CLR} (kJ)	−14	−14	−18
Q _{CLR} /moles H ₂ (kJ/mol)	−2.66	−2.65	−2.57

The results presented indicate that, under autothermal operation, the same H₂ yield can be achieved for the three oxygen carriers. However, while the reduction temperature required for MnWO₄ is 875 °C, it is 100 °C lower for both WO₃ and NiWO₄. Furthermore, it is noteworthy that in the case of NiWO₄, the number of moles of H₂ produced per mole of NiWO₄ reacted is greater than that for MnWO₄ and WO₃. Conversely, for the same H₂ yield, MnWO₄ results in the lowest amount of H₂ produced per mole of OC employed. Regarding net heat, NiWO₄ presents the highest value. However, when comparing the Q_{CLR} per mole of produced H₂, these values become similar.

In summary, to optimize the energy balance, an excess of OC relative to stoichiometric ratios is required in all cases, as higher amounts of OC result in greater heat transfer between the reactors. Regarding operating temperature, the oxidation temperature should be kept as low as possible, while the optimal reduction temperature depends on the specific OC. For MnWO₄, higher reduction temperatures are necessary to enhance OC conversion in the reduction reactor and, consequently, in the oxidation reactor. Conversely, for WO₃ and NiWO₄, lower reduction temperatures are more favorable. However, these conditions do not align with those that maximize hydrogen yield. On one hand, higher amounts of OC promote greater selectivity toward fully oxidized products. Additionally, hydrogen yield presents a maximum at a reduction temperature of approximately 800 °C for all OCs (Figure 4a–c), as lower temperatures lead to reduced CH₄ conversion (Figure S6a–c), while higher temperatures favor H₂O formation due to total oxidation reactions, both of which negatively affect H₂ yield. Although an H₂ yield of 98% can be achieved, this would require external heat input, indicating that autothermal operation would not be feasible. Thus, a compromise must be made between maximizing H₂ yield and optimizing energy performance.

4. Conclusions

This study analyzed the thermodynamic performance of WO₃, MnWO₄, and NiWO₄ as oxygen carriers in chemical-looping reforming for hydrogen production. Complete solid conversion was achieved at lower temperature for WO₃ and NiWO₄ compared to MnWO₄. For WO₃ and NiWO₄, carbon formation was avoided with stoichiometric CH₄:OC ratios at temperature above 875 °C. For MnWO₄, this condition was achieved only with CH₄:OC ratios higher than stoichiometric at temperature above 775 °C. Additionally, stoichiometric CH₄:OC ratios yielded higher H₂ production for all OCs.

The energy balance analysis demonstrated that autothermal conditions were achieved for WO₃ and NiWO₄ at broader temperature ranges compared to MnWO₄. Higher amounts of OC enhance autothermal operation by improving energy transport between reactors, but this comes at the expense of hydrogen yield due to increased complete oxidation reactions. Regarding operating temperature, the oxidation temperature should be kept as low as possible, while the optimal reduction temperature depends on the specific OC.

Reduction temperature significantly affected the energy requirements for all OCs, with lower reduction temperature favoring energy performance in WO_3 and NiWO_4 . MnWO_4 exhibited a distinct behavior due to its temperature-dependent conversion, requiring higher reduction temperature to optimize its energy balance. However, achieving autothermal operation requires compromises in hydrogen yield, as maximizing H_2 production often requires external heat input.

In summary, the thermodynamic framework developed provides valuable insights into the operating conditions for optimal chemical-looping reforming performance. It establishes a foundation for identifying optimal temperature ranges and reactant ratios to enhance the overall performance of the CLR process. Ultimately, the development of effective oxygen carriers requires an interdisciplinary understanding of material science, reaction engineering, and material stability. While thermodynamic analysis serves as a crucial foundation, experimental validation remains indispensable to account for kinetic limitations, diffusion effects, practical operational challenges, and material stability over time.

Supplementary Materials: The following supporting information can be downloaded at <https://www.mdpi.com/article/10.3390/reactions6010005/s1>, Table S1: Enthalpy and Gibbs free energy of formation in standard conditions; Table S2: Coefficients of heat capacity for the equation $c_{p_i} \left[\frac{\text{J}}{\text{mol K}} \right] = a_i + b_i T + c_i T^2 + d_i T^3 + \frac{e_i}{T^2}$ with T in [K]; Figure S1: Enthalpy of reactions against temperature for principal reduction and oxidation reactions; Figure S2: Equilibrium compositions against temperature obtained by Gibbs free energy minimization method for the reaction of 3 moles of CH_4 with (a) 0.50; (b) 0.75; (c) 1.0; (d) 1.25, and (e) 1.50 moles of WO_3 ; Figure S3: Equilibrium compositions against temperature obtained by Gibbs free energy minimization method for the reaction of 3 moles of CH_4 with (a) 0.50; (b) 0.75; (c) 1.0; (d) 1.25, and (e) 1.50 moles of MnWO_4 ; Figure S4: Equilibrium compositions against temperature obtained by Gibbs free energy minimization method for the reaction of 4 moles of CH_4 with (a) 0.50; (b) 0.75; (c) 1.0; (d) 1.25, and (e) 1.50 moles of NiWO_4 ; Figure S5: Gibbs free energy of reactions against temperature for principal reduction and oxidation reactions; Figure S6: CH_4 conversion as a function of reduction temperature, parameterized for different mole amounts of (a) WO_3 ; (b) MnWO_4 ; (c) NiWO_4 ; Figure S7: Equilibrium compositions against temperature obtained by Gibbs free energy minimization method, parameterized for different mole amounts of (a) WO_3 ; (b) MnWO_4 ; (c) NiWO_4 . *The dashed line represents the regeneration of 1.5 moles of OC, the solid line corresponds to 1.25 moles of OC, and the dotted line indicates 1 mole of OC.

Author Contributions: Conceptualization, J.L.v.d.H., M.F.V.G., and F.M.P.; methodology, J.L.v.d.H. and F.M.P.; software, F.S.; validation, J.L.v.d.H.; formal analysis, J.L.v.d.H., M.F.V.G., and F.M.P.; investigation, J.L.v.d.H. and M.F.V.G.; resources, F.P. and G.F.S.; data curation, J.L.v.d.H., M.F.V.G., and F.M.P.; writing—original draft preparation, J.L.v.d.H. and M.F.V.G.; writing—review and editing, F.M.P. and M.N.G.; visualization, M.N.G.; supervision, F.P.; project administration, G.F.S. and F.P.; funding acquisition, F.P. and G.F.S. All authors have read and agreed to the published version of the manuscript.

Funding: This research was funded by the Consejo Nacional de Investigaciones Científicas y Técnicas (CONICET), grant number PIP 0386, and the University of La Plata (UNLP), grant number I-279.

Data Availability Statement: The original contributions presented in the study are included in the article/Supplementary Materials; further inquiries can be directed to the corresponding author.

Acknowledgments: The doctoral fellowship granted by CONICET to J.L.v.d.H. and the postdoctoral fellowship granted by CONICET to F.M.P. are gratefully acknowledged.

Conflicts of Interest: The authors declare no conflicts of interest.

References

1. Yue, M.; Lambert, H.; Pahon, E.; Roche, R.; Jemei, S.; Hissel, D. Hydrogen Energy Systems: A Critical Review of Technologies, Applications, Trends and Challenges. *Renew. Sustain. Energy Rev.* **2021**, *146*, 111180. [CrossRef]
2. Locke, K. The Urgency of Hydrogen: Environmental Issues and the Need for Change. *Futur. Sustain.* **2024**, *2*, 46–58. [CrossRef]
3. IEA The Future of Hydrogen. Available online: <https://www.iea.org/reports/the-future-of-hydrogen> (accessed on 6 June 2024).
4. Diglio, G.; Bareschino, P.; Mancusi, E.; Pepe, F. Novel Quasi-Autothermal Hydrogen Production Process in a Fixed-Bed Using a Chemical Looping Approach: A Numerical Study. *Int. J. Hydrogen Energy* **2017**, *42*, 15010–15023. [CrossRef]
5. Chehade, Z.; Mansilla, C.; Lucchese, P.; Hilliard, S.; Proost, J. Review and Analysis of Demonstration Projects on Power-to-X Pathways in the World. *Int. J. Hydrogen Energy* **2019**, *44*, 27637–27655. [CrossRef]
6. Noor, W.B.; Amin, T. Towards Sustainable Energy: A Comprehensive Review on Hydrogen Integration in Renewable Energy Systems. *Futur. Energy* **2024**, *3*, 1–17. [CrossRef]
7. IRENA International Renewable Energy Agency. Available online: <https://www.irena.org/> (accessed on 6 June 2024).
8. Alirezaei, I.; Hafizi, A.; Rahimpour, M.R. Syngas Production in Chemical Looping Reforming Process over ZrO₂ Promoted Mn-Based Catalyst. *J. CO₂ Util.* **2018**, *23*, 105–116. [CrossRef]
9. U.S. Energy Information Administration. *International Energy Outlook 2021*; U.S. Energy Information Administration: Washington, DC, USA, 2021.
10. Chau, K.; Djire, A.; Khan, F. Review and Analysis of the Hydrogen Production Technologies from a Safety Perspective. *Int. J. Hydrogen Energy* **2022**, *47*, 13990–14007. [CrossRef]
11. De Vos, Y.; Jacobs, M.; Van Der Voort, P.; Van Driessche, I.; Snijkers, F.; Verberckmoes, A.; De Vos, Y.; Jacobs, M.; Van Der Voort, P.; Van Driessche, I.; et al. Development of Stable Oxygen Carrier Materials for Chemical Looping Processes—A Review. *Catalysts* **2020**, *10*, 926. [CrossRef]
12. Shafiefarhood, A.; Hamill, J.C.; Neal, L.M.; Li, F. Methane Partial Oxidation Using FeO_x@La_{0.8}Sr_{0.2}FeO_{3-δ} Core-Shell Catalyst—Transient Pulse Studies. *Phys. Chem. Chem. Phys.* **2015**, *17*, 31297–31307. [CrossRef] [PubMed]
13. Tang, M.; Xu, L.; Fan, M. Progress in Oxygen Carrier Development of Methane-Based Chemical-Looping Reforming: A Review. *Appl. Energy* **2015**, *151*, 143–156. [CrossRef]
14. Liu, R.; Pei, C.; Zhang, X.; Chen, S.; Li, H.; Zeng, L.; Mu, R.; Gong, J. Chemical Looping Partial Oxidation over FeWO_x/SiO₂ Catalysts. *Chin. J. Catal.* **2020**, *41*, 1140–1151. [CrossRef]
15. Kodama, T.; Ohtake, H.; Matsumoto, S.; Aoki, A.; Shimizu, T.; Kitayama, Y. Thermochemical Methane Reforming Using a Reactive WO₃/W Redox System. *Energy* **2000**, *25*, 411–425. [CrossRef]
16. Kwak, J.H.; Han, G.Y.; Yoon, K.J. Zirconia-Supported Tungsten Oxides for Cyclic Production of Syngas and Hydrogen by Methane Reforming and Water Splitting. *Int. J. Hydrogen Energy* **2013**, *38*, 8293–8305. [CrossRef]
17. Sim, A.; Cant, N.W.; Trimm, D.L. Ceria-Zirconia Stabilised Tungsten Oxides for the Production of Hydrogen by the Methane-Water Redox Cycle. *Int. J. Hydrogen Energy* **2010**, *35*, 8953–8961. [CrossRef]
18. Huang, Z.F.; Song, J.; Pan, L.; Zhang, X.; Wang, L.; Zou, J.J. Tungsten Oxides for Photocatalysis, Electrochemistry, and Phototherapy. *Adv. Mater.* **2015**, *27*, 5309–5327. [CrossRef]
19. Song, J.; Huang, Z.F.; Pan, L.; Zou, J.J.; Zhang, X.; Wang, L. Oxygen-Deficient Tungsten Oxide as Versatile and Efficient Hydrogenation Catalyst. *ACS Catal.* **2015**, *5*, 6594–6599. [CrossRef]
20. Luo, S.; Zeng, L.; Fan, L.S. Chemical Looping Technology: Oxygen Carrier Characteristics. *Annu. Rev. Chem. Biomol. Eng.* **2015**, *6*, 53–75. [CrossRef]
21. Chen, S.; Zeng, L.; Tian, H.; Li, X.; Gong, J. Enhanced Lattice Oxygen Reactivity over Ni-Modified WO₃-Based Redox Catalysts for Chemical Looping Partial Oxidation of Methane. *ACS Catal.* **2017**, *7*, 3548–3559. [CrossRef]
22. Corbella, B.M.; De Diego, L.F.; García-Labiano, F.; Adánez, J.; Palacios, J.M. Performance in a Fixed-Bed Reactor of Titania-Supported Nickel Oxide as Oxygen Carriers for the Chemical-Looping Combustion of Methane in Multicycle Tests. *Ind. Eng. Chem. Res.* **2006**, *45*, 157–165. [CrossRef]
23. Quddus, M.R.; Hossain, M.M.; De Lasa, H.I. Ni Based Oxygen Carrier over γ -Al₂O₃ for Chemical Looping Combustion: Effect of Preparation Method on Metal Support Interaction. *Catal. Today* **2013**, *210*, 124–134. [CrossRef]
24. Silvester, L.; Antzara, A.; Boskovic, G.; Heracleous, E.; Lemonidou, A.A.; Bukur, D.B. NiO Supported on Al₂O₃ and ZrO₂ Oxygen Carriers for Chemical Looping Steam Methane Reforming. *Int. J. Hydrogen Energy* **2015**, *40*, 7490–7501. [CrossRef]
25. Ramezani, R.; Di Felice, L.; Gallucci, F. A Review of Chemical Looping Reforming Technologies for Hydrogen Production: Recent Advances and Future Challenges. *J. Phys. Energy* **2023**, *5*, 024010. [CrossRef]
26. Nieva, M.A.; Villaverde, M.M.; Monzón, A.; Garetto, T.F.; Marchi, A.J. Steam-Methane Reforming at Low Temperature on Nickel-Based Catalysts. *Chem. Eng. J.* **2014**, *235*, 158–166. [CrossRef]
27. Mohanty, U.S.; Ali, M.; Azhar, M.R.; Al-Yaseri, A.; Keshavarz, A.; Iglauer, S. Current Advances in Syngas (CO + H₂) Production through Bi-Reforming of Methane Using Various Catalysts: A Review. *Int. J. Hydrogen Energy* **2021**, *46*, 32809–32845. [CrossRef]

28. Stobbe, E.R.; De Boer, B.A.; Geus, J.W. Journal of Molecular Catalysis A: Chemical Promotive Effect of Bi Component on Propane Partial Oxidation Over. *Int. J. Hydrogen Energy* **2013**, *148*–149, 1557–1566.
29. Kiani, D.; Sourav, S.; Baltrusaitis, J.; Wachs, I.E. Oxidative Coupling of Methane (OCM) by SiO₂-Supported Tungsten Oxide Catalysts Promoted with Mn and Na. *ACS Catal.* **2019**, *9*, 5912–5928. [[CrossRef](#)]
30. Zhao, K.; Huang, J.; Huang, Z.; Lin, Y.; Zheng, M.; Song, D.; Liu, A.; Wang, X.; Zheng, A.; Zhao, Z. Tungstate Promoted CaMnO₃-Based Core-Shell Redox Catalysts for Efficient Chemical Looping Oxidative Coupling of Methane. *J. Energy Inst.* **2022**, *105*, 273–281. [[CrossRef](#)]
31. Jiang, Z.; Gong, H.; Li, S. Methane Activation over Mn₂O₃-Na₂WO₄/SiO₂ Catalyst and Oxygen Spillover. *Stud. Surf. Sci. Catal.* **1997**, *112*, 481–490.
32. López van der Horst, J.; Pompeo, F. Thermodynamic Analysis of MnWO₄ as an Oxygen Carrier in a Chemical Looping Scheme for Hydrogen Production. *Next Sustain.* **2024**, *3*, 100033. [[CrossRef](#)]
33. Green, D.W.; Perry, R.H. *Perry's Chemical Engineers' Handbook*, 8th ed.; McGraw-Hill: New York, NY, USA, 1984.
34. Materials Project (Materials Explorer). Available online: <https://materialsproject.org/> (accessed on 10 March 2023).
35. Elsevier Knovel Database. Available online: <https://app.knovel.com/kn> (accessed on 3 March 2023).
36. National Institute of Standards and Technology (NIST) Webbook. Available online: <https://webbook.nist.gov/chemistry/> (accessed on 3 March 2023).
37. Golam Mostafa, A.T.M.; Eakman, J.M.; Yarbrow, S.L. Prediction of Standard Heats and Gibbs Free Energies of Formation of Solid Inorganic Salts from Group Contributions. *Ind. Eng. Chem. Res.* **1995**, *34*, 4577–4582. [[CrossRef](#)]
38. Golam Mostafa, A.T.M.; Eakman, J.M.; Montoya, M.M.; Yarbrow, S.L. Prediction of Heat Capacities of Solid Inorganic Salts from Group Contributions. *Ind. Eng. Chem. Res.* **1996**, *35*, 343–348. [[CrossRef](#)]
39. Zafar, Q.; Abad, A.; Mattisson, T.; Gevert, B.; Strand, M. Reduction and Oxidation Kinetics of Mn₃O₄/Mg-ZrO₂ Oxygen Carrier Particles for Chemical-Looping Combustion. *Chem. Eng. Sci.* **2007**, *62*, 6556–6567. [[CrossRef](#)]
40. Kwak, J.H.; Han, G.Y.; Bae, J.W.; Yoon, K.J. Tungsten Oxides Supported on Nano-Size Zirconia for Cyclic Production of Syngas and Hydrogen by Redox Operations. *Korean J. Chem. Eng.* **2014**, *31*, 961–971. [[CrossRef](#)]
41. Sesen, F.E. Practical Reduction of Manganese Oxide. *J. Chem. Technol. Appl.* **2017**, *1*, 3–4. [[CrossRef](#)]
42. Sridhar, S.; Sichen, D.U.; Seetharaman, S. Investigation of the kinetics of reduction of nickel tungstate by hydrogen. *Metall Mater Trans B.* **1994**, *25*, 391–396. [[CrossRef](#)]
43. Bustnes, J.A.; Sichen, D.; Seetharaman, S. Investigation of the Kinetics of Reduction of Manganese Tungstate by Hydrogen. *Scand. J. Metall.* **2000**, *29*, 151–155. [[CrossRef](#)]
44. Ghosh, S.K. Diversity in the Family of Manganese Oxides at the Nanoscale: From Fundamentals to Applications. *ACS Omega* **2020**, *5*, 25493–25504. [[CrossRef](#)] [[PubMed](#)]
45. Deng, X.C.; Kang, X.D.; Cui, J.; Zhang, G.H. Reaction Mechanism and Kinetics of Carbothermal Reduction of WO₃ to Produce WC. *Jom* **2023**, *75*, 872–885. [[CrossRef](#)]
46. Nava Alonso, F.C.; Zambrano Morales, M.L.; Uribe Salas, A.; Bedolla Becerril, J.E. Tungsten Trioxide Reduction-Carburization with Carbon Monoxide-Carbon Dioxide Mixtures: Kinetics and Thermodynamics. *Int. J. Miner. Process.* **1987**, *20*, 137–151. [[CrossRef](#)]
47. Millner, T.; Neugebauer, J. Volatility of the Oxides of Tungsten and Molybdenum in the Presence of Water Vapour. *Nature* **1949**, *163*, 601–602. [[CrossRef](#)]
48. Blackburn, P.E.; Hoch, M.; Johnston, H.L. The Vaporization of Molybdenum and Tungsten Oxides. *J. Phys. Chem.* **1958**, *62*, 769–773. [[CrossRef](#)]
49. Wendel, J. Thermodynamics and Kinetics of Tungsten Oxidation 200 °C–1100 °C. Master's Thesis, Lund University, Lund, Sweden, 2014.
50. Adanez, J.; Abad, A.; Garcia-Labiano, F.; Gayan, P.; De Diego, L.F. Progress in Chemical-Looping Combustion and Reforming Technologies. *Prog. Energy Combust. Sci.* **2012**, *38*, 215–282. [[CrossRef](#)]
51. Khan, M.N.; Shamim, T. Thermodynamic Screening of Suitable Oxygen Carriers for a Three Reactor Chemical Looping Reforming System. *Int. J. Hydrogen Energy* **2017**, *42*, 15745–15760. [[CrossRef](#)]
52. de Diego, L.F.; Ortiz, M.; García-Labiano, F.; Adánez, J.; Abad, A.; Gayán, P. Hydrogen Production by Chemical-Looping Reforming in a Circulating Fluidized Bed Reactor Using Ni-Based Oxygen Carriers. *J. Power Sources* **2009**, *192*, 27–34. [[CrossRef](#)]
53. López-Ortiz, A.; González-Vargas, P.E.; Meléndez-Zaragoza, M.J.; Collins-Martínez, V. Thermodynamic Analysis and Process Simulation of Syngas Production from Methane Using CoWO₄ as Oxygen Carrier. *Int. J. Hydrogen Energy* **2017**, *42*, 30223–30236. [[CrossRef](#)]
54. Jerndal, E.; Mattisson, T.; Lyngfelt, A.; Combustion, C.; After, O. Thermal Analysis of Chemical-Looping Combustion. *Chem. Eng. Res. Des.* **2006**, *84*, 795–806. [[CrossRef](#)]
55. Kang, K.S.; Kim, C.H.; Bae, K.K.; Cho, W.C.; Kim, S.H.; Park, C.S. Oxygen-Carrier Selection and Thermal Analysis of the Chemical-Looping Process for Hydrogen Production. *Int. J. Hydrogen Energy* **2010**, *35*, 12246–12254. [[CrossRef](#)]

56. Cho, P.; Mattisson, T.; Lyngfelt, A. Carbon Formation on Nickel and Iron Oxide-Containing Oxygen Carriers for Chemical-Looping Combustion. *Ind. Eng. Chem. Res.* **2005**, *44*, 668–676. [[CrossRef](#)]
57. Yahom, A.; Powell, J.; Pavarajarn, V.; Onbhuddha, P.; Charojrochkul, S.; Assabumrungrat, S. Simulation and Thermodynamic Analysis of Chemical Looping Reforming and CO₂ Enhanced Chemical Looping Reforming. *Chem. Eng. Res. Des.* **2014**, *92*, 2575–2583. [[CrossRef](#)]
58. Sudha, A.; Mohammad, M.J.; Solly, M.M.; Swaminathan, P. Nickel Tungstate Derived from WO₃ and NiO for Room Temperature CO₂ Sensing. *Appl. Phys. A* **2024**, *130*, 84. [[CrossRef](#)]
59. Dey, S.; Ricciardo, R.A.; Cuthbert, H.L.; Woodward, P.M. Metal-to-Metal Charge Transfer in AWO₄ (A = Mg, Mn, Co, Ni, Cu, or Zn) Compounds with the Wolframite Structure. *Inorg. Chem.* **2014**, *53*, 4394–4399. [[CrossRef](#)]
60. Montemayor, S.M.; Fuentes, A.F. Electrochemical Characteristics of Lithium Insertion in Several 3D Metal Tungstates (MWO₄, M = Mn, Co, Ni and Cu) Prepared by Aqueous Reactions. *Ceram. Int.* **2004**, *30*, 393–400. [[CrossRef](#)]
61. Gattermann, U.; Park, S.H.; Kaliwoda, M. Synthesis and Characterisation of In-Doped MnWO₄-Type Solid-Solutions: Mn_{1-3x}In_{2x}WO₄ (X=0–0.11). *J. Solid State Chem.* **2014**, *219*, 191–200. [[CrossRef](#)]
62. Lautenschläger, G.; Weitzel, H.; Vogt, T.; Hock, R.; Böhm, A.; Bonnet, M.; Fuess, H. Magnetic Phase Transitions of MnWO₄ Studied by the Use of Neutron Diffraction. *Phys. Rev. B* **1993**, *48*, 6087–6098. [[CrossRef](#)]
63. Mancheva, M.N.; Iordanova, R.S.; Klissurski, D.G.; Tyuliev, G.T.; Kunev, B.N. Direct Mechanochemical Synthesis of Nanocrystalline NiWO₄. *J. Phys. Chem. C* **2007**, *111*, 1101–1104. [[CrossRef](#)]
64. Noh, W.; Shin, Y.; Kim, J.; Lee, W.; Hong, K.; Akbar, S.A.; Park, J. Effects of NiO Addition in WO₃-Based Gas Sensors Prepared by Thick Film Process. *Solid State Ionics* **2002**, *152–153*, 827–832. [[CrossRef](#)]
65. Weber, L.; Egli, U. Phase Relationships in the System NiO-WO₃. *J. Mater. Sci.* **1977**, *12*, 1981–1987. [[CrossRef](#)]
66. Ortiz, M.; Abad, A.; De Diego, L.F.; García-Labiano, F.; Gayán, P.; Adánez, J. Optimization of Hydrogen Production by Chemical-Looping Auto-Thermal Reforming Working with Ni-Based Oxygen-Carriers. *Int. J. Hydrogen Energy* **2011**, *36*, 9663–9672. [[CrossRef](#)]

Disclaimer/Publisher's Note: The statements, opinions and data contained in all publications are solely those of the individual author(s) and contributor(s) and not of MDPI and/or the editor(s). MDPI and/or the editor(s) disclaim responsibility for any injury to people or property resulting from any ideas, methods, instructions or products referred to in the content.